



AFCEC-CX-TY-TR-2022-0012

**EXPERIMENTAL STATIC RESISTANCE  
OF COLD-FORMED STEEL ROOF  
TRUSS SYSTEMS**

---

David Michael Treece

Oak Ridge Institute for Science & Education  
(ORISE)

Contract No. ORISE-AFRL-1072-1072-97

May 2022

**DISTRIBUTION STATEMENT A. Approved for public release; distribution  
unlimited. AFCEC-20220027, 23 June 2022**

**AIR FORCE CIVIL ENGINEER CENTER  
READINESS DIRECTORATE**

## **DISCLAIMER**

**Reference herein to any specific commercial product, process, or service by trade name, trademark, manufacturer, or otherwise does not constitute or imply its endorsement, recommendation, or approval by the United States Air Force. The views and opinions of authors expressed herein do not necessarily state or reflect those of the United States Air Force.**

**This report was prepared as an account of work sponsored by the United States Air Force. Neither the United States Air Force, nor any of its employees, makes any warranty, expressed or implied, or assumes any legal liability or responsibility for the accuracy, completeness, or usefulness of any information, apparatus, product, or process disclosed, or represents that its use would not infringe privately owned rights.**

**REPORT DOCUMENTATION PAGE**

*Form Approved  
OMB No. 0704-0188*

The public reporting burden for this collection of information is estimated to average 1 hour per response, including the time for reviewing instructions, searching existing data sources, gathering and maintaining the data needed, and completing and reviewing the collection of information. Send comments regarding this burden estimate or any other aspect of this collection of information, including suggestions for reducing the burden, to Department of Defense, Washington Headquarters Services, Directorate for Information Operations and Reports (0704-0188), 1215 Jefferson Davis Highway, Suite 1204, Arlington, VA 22202-4302. Respondents should be aware that notwithstanding any other provision of law, no person shall be subject to any penalty for failing to comply with a collection of information if it does not display a currently valid OMB control number.

**PLEASE DO NOT RETURN YOUR FORM TO THE ABOVE ADDRESS.**

1. REPORT DATE (DD-MM-YYYY) 05-2022		2. REPORT TYPE Thesis/Dissertation		3. DATES COVERED (From - To)	
4. TITLE AND SUBTITLE Experimental Static Resistance of Cold-Formed Steel Roof Truss Systems				5a. CONTRACT NUMBER ORISE-AFRL-1072-1072-97	
				5b. GRANT NUMBER	
				5c. PROGRAM ELEMENT NUMBER	
6. AUTHOR(S) David Michael Treece				5d. PROJECT NUMBER	
				5e. TASK NUMBER	
				5f. WORK UNIT NUMBER	
7. PERFORMING ORGANIZATION NAME(S) AND ADDRESS(ES) Oak Ridge Institute for Science & Education (ORISE)				8. PERFORMING ORGANIZATION REPORT NUMBER	
9. SPONSORING/MONITORING AGENCY NAME(S) AND ADDRESS(ES) Air Force Civil Engineer Center Readiness Directorate Requirements and Acquisition Division 139 Barnes Drive, Suite 1 Tyndall Air Force Base, FL 32403-5323				10. SPONSOR/MONITOR'S ACRONYM(S) AFCEC/CXA	
				11. SPONSOR/MONITOR'S REPORT NUMBER(S) AFCEC-CX-TY-TR-2022-0012	
12. DISTRIBUTION/AVAILABILITY STATEMENT Distribution Statement A: Approved for public release; distribution unlimited.					
13. SUPPLEMENTARY NOTES					
14. ABSTRACT This study aims to analyze the full static resistance of full-scale cold-formed steel trusses commonly used in the industry and identify associated failure modes in order to more accurately predict dynamic response with simplified methods. Sixteen unique truss designs were tested under quasi-static loading up to ultimate failure using a mechanical testing system. Three select designs will be discussed in this thesis. A simplified finite element analysis was performed using SAP2000 non-linear analysis and compared to experimental results. Experimental results show that truss performance and absorbed energy are significantly affected by the truss configuration and thickness of truss elements. Results of this study will be used to validate advanced numerical models. The quantifiable application of system capacities will improve future designs of building systems and lead to a more safe and resilient infrastructure.					
15. SUBJECT TERMS Truss systems, steel roof					
16. SECURITY CLASSIFICATION OF:			17. LIMITATION OF ABSTRACT	18. NUMBER OF PAGES	19a. NAME OF RESPONSIBLE PERSON
a. REPORT	b. ABSTRACT	c. THIS PAGE			Kevin Wise
U	U	U	UU	78	19b. TELEPHONE NUMBER (Include area code) 405 535 3638

# Experimental Static Resistance of Cold- Formed Steel Roof Truss Systems

A Thesis Presented to the Faculty of the Graduate School of the  
University of Missouri-Columbia

---

In Partial Fulfillment of the Requirements for the Degree

Master of Science In

Civil and Environmental Engineering

---

By

David Michael Treece

Dr. Hani Salim, Thesis Supervisor

APRIL 2022

The undersigned, appointed by the dean of the Graduate School, have examined the thesis entitled

“Experimental Static Resistance of Cold-Formed Steel Roof Truss Systems”

presented by David Michael Treece,

a candidate for the degree of Master of Science in Civil and Environmental Engineering, and hereby certify that, in their opinion, it is worthy of acceptance.

---

Professor Hani Salim

---

Professor John Gahl

---

Professor Alaaeldin Elsis

## Acknowledgements

I would like to thank my committee chair and faculty advisor, Professor Hani Salim, for his encouragement and wisdom throughout my time in graduate school, and during the writing of this thesis.

I would like to thank the members of the research team, Dr. Aaron Saucier, Richard Oberto, and Chris Strehl for their guidance in the research facility. I also want to express my appreciation for my fellow graduate student, Mohamed Elsayi, who led me through the process and generously offered his time and talents to help me succeed.

I would like to offer my sincere appreciation for my thesis committee, Dr. Alaaeldin Elsayi and Dr. John Gahl, for their time, comments, and continued interest in this research. I would also like to thank Dr. Elsayi for his assistance in static testing, data analysis, and literature review, and numerical analysis.

Finally, I would like to thank Battelle Memorial Institute for providing financial support and valued collaboration with the Air Force Civil Engineer Center (AFCEC) at Tyndall Air Force Base and the United States Department of State. Special thanks to Mr. Michael Newberry and Mr. Kevin Wise for their guidance and support throughout the project.

# Table of Contents

List of Figures .....	iii
List of Tables .....	iv
Abstract .....	v
1. Introduction.....	1
1.1. Motivation .....	4
1.2. Thesis overview.....	5
2. Literature Review.....	6
2.1. Blast Analysis techniques.....	6
2.2. Previous Research .....	8
2.3. Blast loads on building with a gable roof.....	14
3. Experimental Test Setup.....	15
3.1. Loading Mechanism.....	15
3.2. Test Matrix .....	19
3.3. Specimen Preparation.....	22
3.4. Loading Scenario.....	27
4. Experimental Results .....	29
4.1. AG36-D35 .....	29
4.2. AG48-D35 .....	36
4.3. AG48-D57 .....	42
4.4. Parametric Study .....	47
6. Conclusion and Recommendations.....	51
6.1. Conclusion.....	51
6.2. Recommendations .....	52
7. References .....	54
Appendix A.....	55
Appendix B .....	62

# List of Figures

Figure 1: Idealized Blast Pressure History.....	2
Figure 2: Simplified Equivalent Load History (Bondok et al., 2021) .....	3
Figure 3: Loading Tree Test Setup (McClendon 2007).....	9
Figure 4: Midpoint Static Response of a 16K5 Joist Compared with existing Methods (McClendon 2007).....	10
Figure 5: Testing of Small Scale CFS Truss (Clayton 2017) .....	11
Figure 6: Deflection Response Comparison at Mid-point (Bondok et al., 2018).....	12
Figure 7: Loading Tree Concept.....	15
Figure 8: Loading Mechanism Structure .....	16
Figure 9: Pulley Assembly.....	17
Figure 10: Loading Mechanism Setup.....	18
Figure 11: Aegis Truss System Geometries.....	21
Figure 12: Web Member Cross-Sections of Aegis Designs. ....	21
Figure 13: Cold Formed Web Members .....	22
Figure 14: Truss Assembly .....	22
Figure 15: Swiftclip Bracing Angles .....	23
Figure 16: Fully Assembled Specimen.....	24
Figure 17: Lateral Restraint System. ....	24
Figure 18: Instrumentation Placement.....	25
Figure 19: Data Acquisition System.....	26
Figure 20: Typical End Bearing Connection .....	27
Figure 21: Blast Wave Pressures Plotted Against Time. ....	28
Figure 22: Load vs. Displacement of AG36-D35.....	30
Figure 23: Distortion of Compression Chords in AG36-D35.....	31
Figure 24: Local Buckling of Tension Chord at Joint Q (AG36-D35).....	32
Figure 25: Initial Deformation of Compression Diagonal at Joint QS (AG36-D35) .....	33
Figure 26: Partial Failures in Web Element Connections (AG36-D35).....	34
Figure 27: Bearing Connection Failure at RN (AG36-D35) .....	35
Figure 28: Bearing Connection at Joint RS (AG36-D35).....	36
Figure 29: Load and Energy vs Displacement (AG48-D35) .....	37
Figure 30: Global Failure of Specimen (AG48-D35).....	38
Figure 31: Rupture of Diagonal at Joint AN (AG48-D35).....	39
Figure 32: Bending of Tension Chords at Joint Q (AG48-D35) .....	40
Figure 33: West End Vertical Distortion (AG48-D35).....	40
Figure 34: Partial Tearing in Tension Chord at Joint QN (AG48-D35).....	41
Figure 35: Connection Failure Between Tension Chord and End Vertical at Joint RN (AG48-D35).....	41
Figure 36: West Quarter of Specimen During Failure (AG48-D35) .....	42
Figure 37: Load and Energy vs Displacement (AG48-D57) .....	43
Figure 38: Global Failure of Specimen.....	43
Figure 39: Initial Tension Chord Deformation (AG48-D57) .....	45
Figure 40: Beginning of Tension Chord Separation (AG48-D57) .....	45

Figure 41: Full Tension Chord Separation.....	46
Figure 42: Cutting of Tension Chord Section (AG48-D57).....	46
Figure 43: Compression Chord Bending (AG48-D57).....	47
Figure 44: Load vs Displacement Comparison.....	48
Figure 45: Energy vs Displacement Comparison.....	49
Figure 46: Specimen Setup - Longitudinal View.....	55
Figure 47: Specimen Setup - Plan View.....	55
Figure 48: Specimen Setup - Quarter Span.....	56
Figure 49: Specimen Setup - End Panel.....	56
Figure 50: Specimen Setup - End Bearing.....	57
Figure 51: Compression Cord Sheathing.....	57
Figure 52: #10-16 Tek Screws.....	58
Figure 53: Hat Channel for Bracing.....	58
Figure 54: Displacement Potentiometer Placement.....	59
Figure 55: Straing Gauge Placement.....	59
Figure 56: Pulley and Cable Elevation View.....	60
Figure 57: Caster Wheel Placement Elevation.....	60
Figure 58: Caster Wheel Placement Plan.....	61
Figure 59: Load vs Time (AG36-D35).....	62
Figure 60: Load vs Time (AG48-D35).....	62
Figure 61: Load vs Time (AG48-D57).....	63
Figure 62: Load vs Displacement (AG36-D35).....	63
Figure 63: Load vs Displacement (AG48-D35).....	64
Figure 64: Load vs Displacement (AG48-D57).....	64
Figure 65: Load vs Energy (AG36-D35).....	65
Figure 66: Load vs Energy (AG48-D35).....	65
Figure 67: Load vs Energy (AG48-D57).....	66
Figure 68: Load vs Strain (AG36-D35).....	66
Figure 69: Load vs Strain (AG48-D35).....	67
Figure 70: Load vs Strain (AG48-D57).....	67

## List of Tables

Table 1: CFS roof specimen specifications. ....	20
Table 2: Parametric Data.....	47

# Experimental Static Resistance of Cold-Formed Steel Roof Truss Systems

David Michael Treece

Dr. Hani Salim, Thesis Supervisor

## Abstract

Critical infrastructure vulnerable to attack or located in areas of high threat requires increased protection. U.S. facilities at home and abroad have seen disruption and destruction due to lack of capability to fully resist attack. Increasing effort to improve the building structure, particularly building envelope systems, can improve the life-safety and continued operability of critical infrastructure under adverse circumstances. The popularity of cold-formed steel (CFS) building components has seen a sharp rise in recent years due to its low cost, high strength, ease of construction, and design flexibility. Despite its extensive use, no design criteria exist for the design of cold-formed steel roof systems under blast load. While extensive studies have been conducted on blast load on CFS walls, sufficient research has not been done to develop adequate design procedures for CFS roof systems. Past research has explored the behavior of these truss systems up to ultimate capacity, but the full inelastic behavior was not fully captured. Since many structures are allowed to sustain permanent deformations in blast scenario, it is critical to the safety of building occupants to fully understand the non-linear response of building envelope systems. Dynamic testing and numerical analysis are uneconomical and tedious for every design variation, so the simplified single degree of freedom (SDOF) approach to dynamic analysis is commonly used to project blast resistance of complicated

structural systems. In order to perform the SDOF analysis, a static resistance function is required.

This study aims to analyze the full static resistance of full-scale cold-formed steel trusses commonly used in the industry and identify associated failure modes in order to more accurately predict dynamic response with simplified methods. Sixteen unique truss designs were tested under quasi-static loading up to ultimate failure using a mechanical testing system. Three select designs will be discussed in this thesis. A simplified finite element analysis was performed using SAP2000 non-linear analysis and compared to experimental results. Experimental results show that truss performance and absorbed energy are significantly affected by the truss configuration and thickness of truss elements. Results of this study will be used to validate advanced numerical models. The quantifiable application of system capacities will improve future designs of building systems and lead to a more safe and resilient infrastructure.

# 1. Introduction

Throughout the history of buildings design and construction, the industry has pushed the envelope to produce taller structures and longer spans, all while increasing efficiency and economy. Human safety, however, remains the chief concern of structural design. The goals for the current research are no different than that of any structural research conducted in past years: to create structures that provide ideal ratios of strength to cost while ensuring the safety and protection of the public. In recent years, cold-formed steel has risen to provide the high strength to cost relationship that the industry craves. In order to establish this new material as a prime candidate for affordability and constructability, scientific research is necessary to understand its behavior in any given loading scenario. While much research has been done into the performance of cold-formed stud walls under blast loading, uncertainty remains in the performance of cold-formed roof truss systems under explosive impulse. In the last twenty years, open web steel joists have grown in popularity for framing roof systems of one or two-story buildings with relatively regular geometry. The rise in popularity is due to their low cost-to-weight ratio and high ductility.

Recently, cold-formed steel trusses have increased in frequency for similar reasons. The problem with both is that the post-buckling response of such systems is not well understood. For blast resistant design, in particular, it is important to understand how the static and dynamic resistance functions will behave past the linear elastic range. Without this, it is impossible to predict the response under blast loading. For any given structure,

the dynamic response can be analyzed using the equation of motion as shown in equation 1.1. This equation can be solved with a variety of numerical methods.

$$M\ddot{y} + R = F(t) \quad (1.1)$$

where  $M$  = mass  
 $R$  = resistance  
 $F(t)$  = applied load

The mass of a structure is easy to determine, however, the other two parameters are not. The main issue that must be addressed in research is the design method for calculating blast load on a roof system. Much research has been conducted on blast load interaction with walls and columns, leading to well-established industry codes and standards for calculating accurate design loads. Blast load on roof systems, however, is dynamic, nonuniform, and non-simultaneous. The current industry standard for calculating a design load for a blast on roof systems utilizes the equivalent force procure (UFC, 2014)

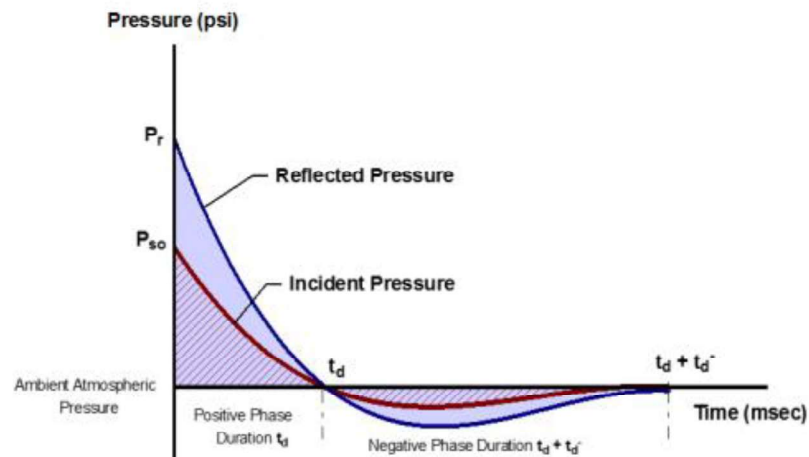


Figure 1: Idealized Blast Pressure History

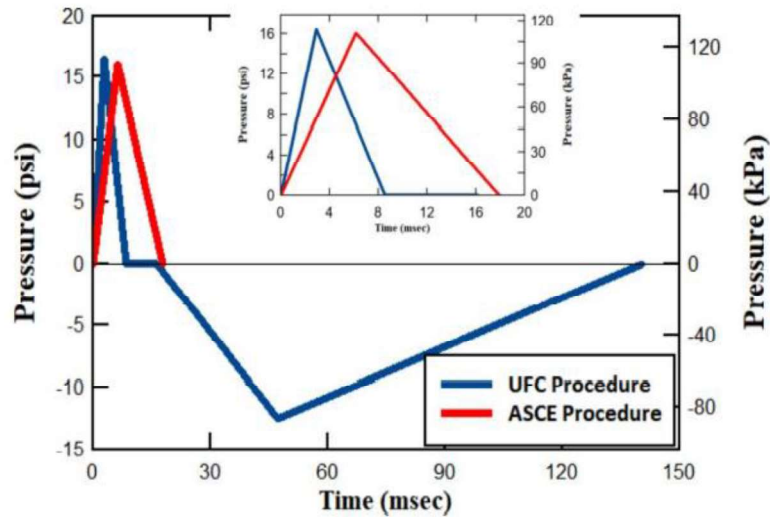


Figure 2: Simplified Equivalent Load History (Bondok et al., 2021)

This procedure, as shown by many studies in the last twenty years, significantly overestimates the blast response (McClendon, 2007). The procedure approximates the blast load as a triangular load history with a steep linear rise, and a linear decay (Figure 2). The issue is that it does not adequately represent the duration or magnitude of a real blast (Figure 1). It also assumes a uniform spatial application of the load, causing blast loads applied to beams running perpendicular to the shock front to be overestimated. Several studies have compared these procedures to experimental blast scenarios, as well as numerical models in order to suggest a better approach for calculating design loads (Esper, 2004; Gannon C. J. et al., 2012; McClendon, 2007; Nourzadeh et al., 2017). See chapter 2 for a more in-depth discussion of previous research.

The other is the issue of resistance, which is the focus of this research. The resistance of many structural systems used in the construction of roof slabs is known. In addition to concrete and hot-rolled steel members, open web steel joists are also common roof

components. Current techniques used in design assume a linear elastic, pure plastic load-deflection curve. It is believed that such truss systems exhibit different failure modes than those currently used in the design. Due to their high use in military and commercial buildings, current design practices should be researched and improved.

Cold-formed steel (CFS) trusses are especially difficult to investigate because of inconsistencies in section geometry between manufacturers. Unlike open web steel joists (OWSJ), each CFS truss manufacturer has its own proprietary section geometry, resulting in unique failure modes and behavior for each truss design. Unlike conventional steel sections or reinforced concrete beams, steel trusses do not have a consistent moment of inertia along the span, making it difficult to determine the resistance functions of the countless joist configurations.

## **1.1. Motivation**

The overall motivation of this research is to develop analysis and design procedures for cold-formed steel (CFS) roof truss systems under blast load. This will be achieved via two distinct tasks:

- Quasi-static experimental testing of full-scale CFS roof trusses
- Numerical modeling and evaluation of roof truss systems using SAP 2000 non-linear analysis

The goal of the experimental static testing is to evaluate the resistance and failure mechanisms of truss systems with varying depths, manufacturers, and configurations.

The post-buckling response will be monitored throughout testing until ultimate failure

occurs. The experimental evaluation also serves to validate numerical models which will ultimately be used to create a graphical design tool.

## **1.2. Thesis overview**

This thesis will consist of 6 chapters. Chapter two gives a review of relevant literature from the past twenty years of experimental testing. The review examines journal articles on experimental or numerical evaluation of cold-formed roof truss systems and wall studs subject to blast load. It also includes an explanation of the current knowledge of blast load and wave propagation over a low-height roof structure.

Chapter 3 presents a new and unique method of testing trusses. It discusses the design and construction of a full-scale testing mechanism for testing trusses of varying size and configuration using a single load source. The chapter also discusses the testing matrix, manufacturing of samples, and testing instrumentation.

Chapter 4 presents the static testing of the full-scale CFS trusses examined in this research. The chapter discusses experimental results and gives observations pertaining to failure modes and blast resistance. Chapter 5 presents the numerical modeling technique and discusses the results of a non-linear SAP analysis. Results of the numerical analysis are compared to the static experimental results. Chapter 6 summarizes the analysis of the research, gives the main conclusions, and presents recommendations for future work.

## 2. Literature Review

To effectively evaluate the response of cold-formed roof trusses under blast load, it is necessary to understand the influence of blast on roof structures. This chapter discusses current techniques for determining blast effects. Additionally, design methods for roof structures will be introduced and previous research on the experimental determination of static resistance functions of roof systems will be explored.

### 2.1. Blast Analysis techniques

Standard criteria for the approximation of blast load was first published by the Department of the Army in 1959 with the title “Structure to Resist the Effects of Accidental Explosions.” The revised edition, published in 1990 as TM 5-1300, became widely used as a tool for protective design of structures against explosive threats. More recently, the United Facilities Criteria (UFC) manual has surpassed ARMY TM 5-1300 as the industry standard for protective design methods. UFC 3-240-02 prescribes reasonable methods for blast-resistant design based on extensive research, including numerous small and full-scale dynamic tests (UFC 3-340-02S, 2014).

The single degree of freedom technique (SDOF) utilizes widely accepted assumptions for the prediction of blast response. It is the most widely used and practical method for blast design and analysis. The method idealizes a structure as a SDOF system with a lumped mass and spring system. Transformation factors,  $K_L$  and  $K_M$ , are used to find the equivalent lumped mass,  $M_e$ , equivalent resistance,  $R_e$ , and equivalent load,  $F_e$  (Biggs, 1964). The SDOF method is explained in detail in the 1964 treatise on structural

dynamics by John Biggs, titled “Introduction to Structural Dynamics.” When an external dynamic load is applied to the structure, its response is controlled by the equation of motion, **Eq. 1**. By idealizing the system as a SDOF, the response can then be characterized by **Eq. 2** which is derived by taking the sum of forces on the system in the y-direction. **Eq. 2**, also introduces the use of the load transformation factor,  $K_L$ , and the mass transformation factor,  $K_M$ , to perform the idealization process. **Eq. 3** is derived by dividing **Eq. 4** by  $K_L$  and introduces the load-mass transformation factor,  $K_{LM}$ .

$$\underbrace{F(t)}_{\text{applied force}} - \underbrace{K \cdot y(t)}_{\text{resistance force}} = \underbrace{m a}_{\text{inertia force}} \quad \text{Eq. (1)}$$

$$\underbrace{K_L F(t)}_{F_e(t)} - \underbrace{(K_L K)}_{K_e} y(t) = \underbrace{K_M m a}_{m_e} \quad \text{Eq. (2)}$$

$$F(t) - K \cdot y(t) = \underbrace{K_{LM}}_{K_M/K_L} m a \quad \text{Eq. (3)}$$

$$F(t) - SRF(y) = K_{LM} m a \quad \text{Eq. (4)}$$

Where:

$F(t)$  = applied external dynamic load, which is a function of time

$K$  = stiffness of structure

$y(t)$  = deflection of structure, which is a function of time

$m$  = mass of structure

$a$  = acceleration

$K_M$  and  $K_L$  = equivalent mass and equivalent load factors, respectively.

$F_e(t)$  = equivalent dynamic load

$m_e$  = equivalent mass of structure

$K_e$  = equivalent stiffness of structure

Finite element analysis can be used to predict and analyze structural blast response. Finite element methods do not have limitations regarding simulation of the propagated blast

wave or identification of the static resistance. However, it requires experience, skill, and importantly verification of the model and analytical method.

## 2.2. Previous Research

(Esper, 2004) investigated building damage caused by attacks through on-site and laboratory testing of structural elements. From the analyses, Esper concluded that finite element analysis is a more economic approach to study blast effects and more adaptable to various applications. (Gannon C. J. et al., 2012) studied the applicability of using equivalent uniform loads to model blast loads on long-span girders with spans ranging from 80-160 ft. The study proposed an alternative method to model blast load for long-span girders that offers increased accuracy and is suitable for initial design. A thesis by Mark McClendon in 2007 titled *Blast Resistant Design for Roof Systems* evaluated the adequacy of various industry methods for calculating the resistance function of open web steel joists, such as conventional engineering calculations and the single degree-of-freedom Blast Effects Design Spreadsheet from the DoD, (SBEDS) (McClendon, 2007). The study found that industry methods for calculating the resistance function of steel joists severely overestimate the resistance of steel joists. McClendon used a loading tree to test three unique OWSJ configuration under uniform load, in order to determine the static resistance and evaluate failure modes (Figure 3).



Figure 3: Loading Tree Test Setup (McClendon 2007)

While experimental initial stiffness (in the linear elastic portion) and ultimate resistance are similar to the conventional methods, they do not consider the effects of various failure modes in the truss members. While the assumed Load-deflection curve is linear elastic, then perfectly plastic, the reality is that the load will drop every time a truss web member buckles, or a connection fails. Displacement will continue until the end connection fails, resulting in a load deflection curve that is far from the calculated resistance (Figure 4)

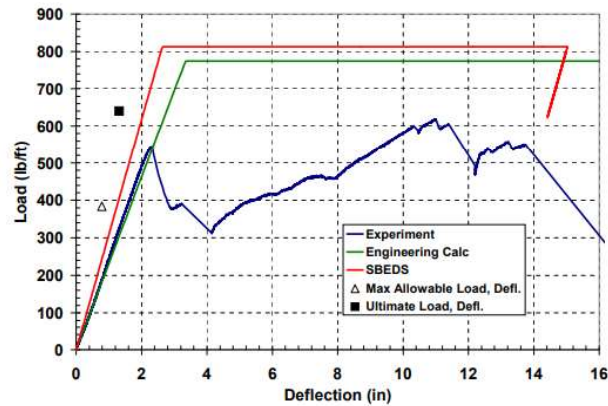


Figure 4: Midpoint Static Response of a 16K5 Joist Compared with existing Methods  
(McClendon 2007)

The study also found that the equivalent load procedure (DAHS) does not adequately predict the blast response at roof level, compared to either experimental blast pressures, or numerically computed values. This is because the DAHS method approximates that blast load as a triangular impulse with linearly increasing load and linearly decay, applied equally to the entire length of the beam. In reality, the blast load will have an instantaneous rise, followed by a logarithmic decay and a negative pressure phase of longer duration. The load will have a greater effect on the end of the beam closer to the blast. The study concluded that more research was needed to adequately determine the resistance function of OWSJ and to calculate with more accuracy the blast load experienced by the roof system. Like open web steel joists, cold-formed steel joists are growing in popularity due to low cost to weight ratio. However, their response to a blast scenario is even harder to predict due to variation in proprietary section properties between manufacturers, and the lack of research on the post-linear response.

Like the McClendon Report, (Clayton & Salim, 2017) attempted to experimentally determine the static resistance function of small scale CFS trusses, as well as the response of roof members to a dynamic blast load. Clayton also evaluates the efficacy of the current equivalent blast load procedure. The study used Finite Element software ABAQUS 6.11 to model the response of a typical roof member under blast loading. Clayton compared a typically observed loading shape with an instantaneous peak and logarithmic decay, followed by a negative pressure phase of longer duration, to the equivalent load methods found in UFC and ASCE. The ABAQUS model was verified with the Newark  $\beta$  numerical integration time-step solution method. The comparison concluded that both the ASCE and UFC methods produce a significant error in estimation of the first and second peak dynamic responses, with error ranging from 50 to 80% depending on scaled standoff distance and member length. However, no correlation could be made between error and scaled distance or length.

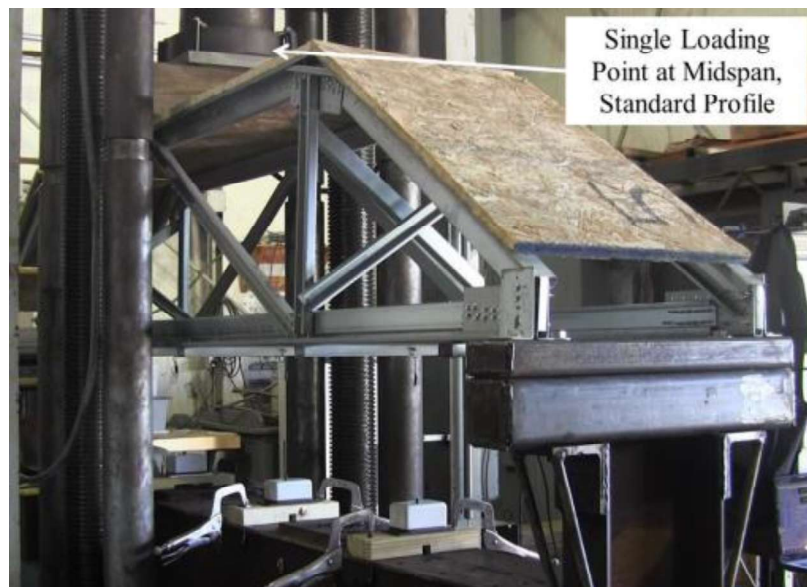


Figure 5: Testing of Small Scale CFS Truss (Clayton 2017)

Experimental results from the small-scale truss testing (Figure 5) showed that resistance was greater when failure occurred as local buckling opposed to buckling of a web member. This is because a system can easily redistribute load when local buckling occurs around a connection, allowing the structure to develop post-buckling strength. When a web member fails, the structure experiences a large release of energy and steep drop in resistance. A 2018 paper by Salim and Bondok titled *Dynamic response of roof truss systems under blast loading* uses data from the first two papers, along with experimental data from dynamic field tests to continue to evaluate the efficacy of the equivalent load procedure (Bondok et al., 2018). Conclusions were similar to those of McClendon and Clayton. The researchers used the results of a 2007 dynamic field test to verify the dynamic response prediction of a FEM model using ABAQUS 6.11. They then compared the predicted response with the response calculated by ASCE and UFC procedures (Figure 6).

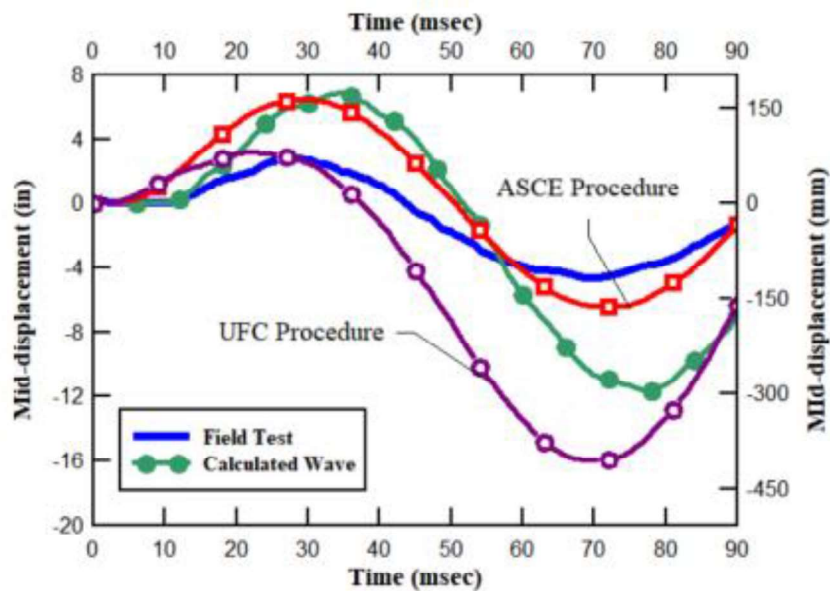


Figure 6: Deflection Response Comparison at Mid-point (Bondok et al., 2018)

While the ABAQUS model was verified by the results, the ASCE and UFC methods both produced significant error. The ASCE method produced less error due to the exclusion of the negative pressure phase, although both methods consistently underpredicted the maximum response. The overestimation of the negative pressure phase in the UFC procedure caused the first phase peak deflection to be lower than its ASCE counterpart. Results of the 2007 study on static resistance of OWSJ (McClendon, 2007) were used to develop the numerical model for predicting the static resistance function of OWSJ . Trials showed that ABAQUS 6.11 accurately predicted the static and dynamic resistance of the three OWSJ configurations tested in 2007.

(Nourzadeh et al., 2017) evaluate methods for analyzing roof beams that run perpendicular to the shock front. In other words, beams in which the blast response varies along the span can create challenges in analysis that are not addressed in current ASCE, UFC or TM (Department of the Army) design methods. The paper compares responses of a wide-flanged simply supported steel roof beam with a blast wave traveling down the span length using conventional design procedures, SDOF analysis, and MDOF analysis with OpenSEES FEM software. The study analyzed various blast wavelengths and span lengths. The study concluded that UFC and ASCE equivalent loading methods overestimate maximum displacements by up to 800%, while the Department of the Army's TM 5-855 method overestimated ultimate deflection by up to 70% of the MDOF method. It should also be noted that the difference between method results increases with the magnitude of the blast.

### **2.3. Blast loads on building with a gable roof**

A 2021 Study by (Xiao et al., 2021) titled *Investigations of blast loads on a two-storied building with a gable roof: Full-scale experiments and numerical study* analyzes the effect of blast load on two story structures with gabled roofs. The researchers constructed a two-story reinforced concrete and masonry structure with a 36 deg sloped roof and gable, having an overhang on one side. The team created five blast scenarios, placing charges on various sides of the building and at various distances. A numerical model was created to further investigate the effect of overhang length and roof slope on peak impulse and overpressure. The numerical model was verified with experimental data. From the experimental and numerical results, it was concluded that higher peak overpressures are observed with longer overhang lengths and steeper roof slopes. It was also concluded that increased overhang lengths cause higher peak impulse, but roof slope has almost no effect on peak impulse.

# 3. Experimental Test Setup

## 3.1. Loading Mechanism

In previous experimental truss testing, such as the 2017 study by Bondok and Salim, a loading tree has always been used to load the specimens such as the one in Figure 7. In this configuration, a single hydraulic actuator applies an upward force to the loading tree, which distributes the load to rows of load spreaders until the desired number of point loads is reached.



Figure 7: Loading Tree Concept

The drawbacks of this approach are clear. The loading configuration is difficult to change for varying truss dimensions, truss size is limited due to the need to progressively spread the load away from the actuator, and displacement range is limited by the actuator. A new loading mechanism was developed at the University of Missouri Remote Testing Facility (RTF) with the objective of easily accommodating variable truss configurations. The system can produce multiple equal point loads as needed and achieves a displacement-controlled loading condition. Displacement range is limited only by the distance from the



The mechanism features 5 main components: a steel loading structure, supporting frames, a pulley and cable system, a motor and drum, and a data acquisition system. The supporting structure is shown in Figure 8. The data acquisition system was designed with capacity to host 10 strain gauges, 6 displacement potentiometers, and 8 load cells. Load cells are positioned between the loading structure and the pulley assemblies such that they are loaded equally to the point load by the downward force on the pulleys. The top flange of the loading structure girder features holes spaced at regular intervals, while the pulley assemblies are mounted on slotted plates. This allows the pulleys to be easily moved to any position.



Figure 9: Pulley Assembly

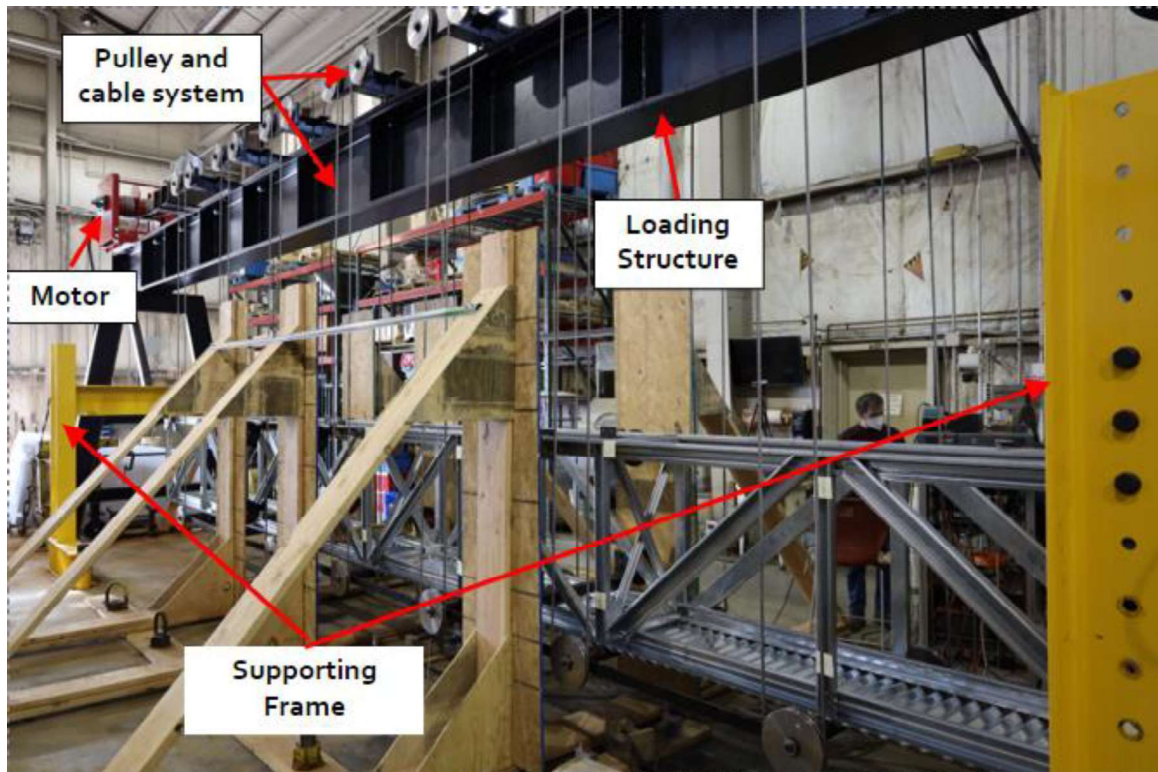


Figure 10: Loading Mechanism Setup

Similar to open web steel joists, CFS truss manufacturers produce pre-designed truss configurations for use in a roofing application. However, unlike OWSJ truss manufacturers, CFS member sections are not standardized by any national body. This means that every CFS truss manufacturer has their own proprietary section design. In order to guarantee the verity of the CFS truss systems, products of two different steel truss fabricators were considered in this research. The first group consists of 10 samples with three truss heights and various sections, which were provided by Aegis Metal Framing. The second group also consists of 10 samples with five truss heights and various sections that were provided by TrusSteel Metal Framing. The twenty large-scale 30 ft long trusses' steel members were assembled in the Remote Testing Facility (RTF) at the University of Missouri-Columbia. Specimens' specifications are given in Table 1.

## 3.2. Test Matrix

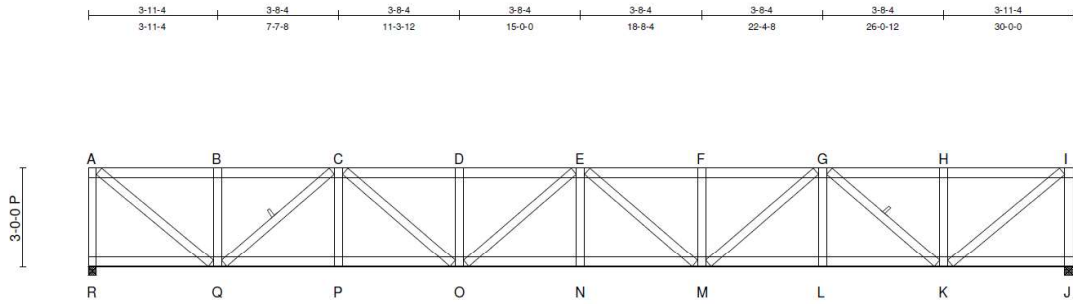
A total of 16 unique truss configurations were tested at the University of Missouri Remote Testing Facility (RTF). Two identical samples were acquired and tested for each design to ensure reasonable results. Designs 1-8 were furnished by Aegis Metal Framing and manufactured by students at the MU RTF. Designs 9-16 were furnished by Alpine TrusSteel and delivered to the RTF pre-assembled. This paper will focus on three designs from Aegis: AG36-D35, AG48-D35, and AG48-D57. The first two letters of the truss designation refer to the manufacturer/designer, ie. AG for Aegis. The following number refers to the truss height in inches, and the final letter and number indicate the section type and thickness, ie. D-type section of thickness 0.035 inches. Section geometries for the specimens that will be discussed are shown in Figure 12. Table 1 shows the complete testing matrix for Aegis and TrusSteel specimens. Typical geometries for Aegis trusses are shown in Figure 11.

Table 1: CFS roof specimen specifications.

#	Truss Sample	Upper Chord	Lower Chord	Main Web	K*, lb/in
1	AG36-C35	35 USC 035	35 USC 035	30 USW 035	6406.154
2	AG36-C57	35 USC 057	35 USC 046	30 USW 035	8623.188
3	AG48-C35	35 USC 035	25 USC 035	30 USW 035	9683.721
4	AG48-C57	35 USC 057	35 USC 035	30 USW 035	13282.14
5	AG36-D35	35 USD 035	35 USD 035	25 USWD 035	7547.541
6	AG36-D57	35 USD 057	35 USD 046	25 USWD 035	10493.33
7	AG48-D35	35 USD 035	25 USD 035	25 USWD 035	13095.45
8	AG48-D57	35 USD057	35 USD 035	25 USWD 035	15740
9	TS24-28-275	28 TSC 275	28 TSC 275	33 W 0.75x1.5	1127.82
10	TS48-28-275	28 TSC 275	28 TSC 275	33 W 0.75x2.25	3260.87
11	TS18-43-275	43 TSC 275	43 TSC 275	33 W 0.75x2.25	903.61
12	TS36-43-275	43 TSC 275	43 TSC 275	33 W 0.75x1.5	2884.62
13	TS18-33-300	33 TSC 3.00	33 TSC 300	33 W 1.5x1.5	862.07
14	TS48-33-300	33 TSC 3.00	33 TSC 300	33 W 1.5x1.5	4687.50
15	TS12-54-300	54 TSC 300	54 TSC 300	33 W 1.5x1.5	547.45
16	TS48-54-300	54 TSC 300	54 TSC 300	33 W 1.5x1.5	6000.00

\*K: Manufacturer Design Sheet Stiffness.

a) 3 ft Truss Geometry (AG36)



b) 4 ft Truss Geometry (AG48)

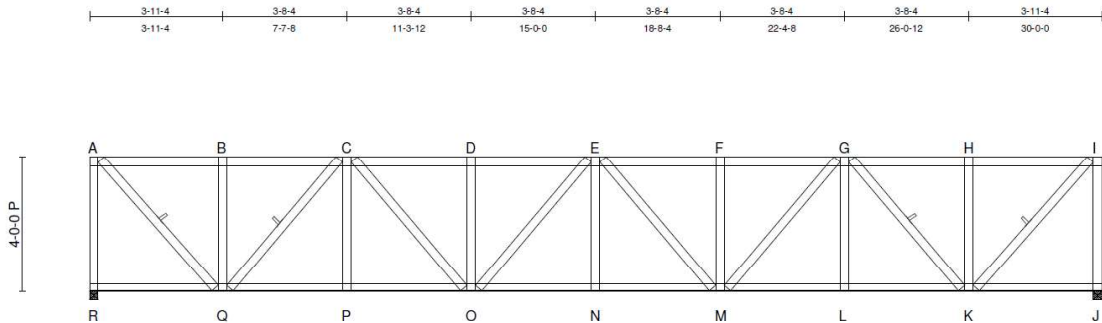


Figure 11: Aegis Truss System Geometries.

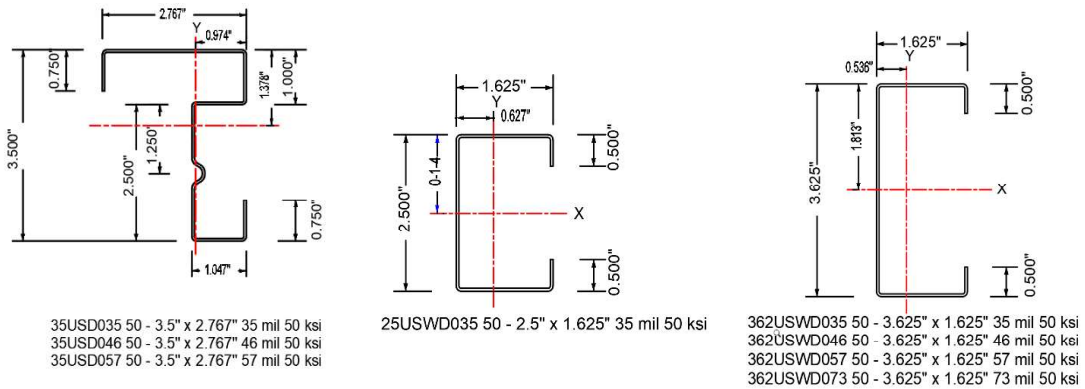


Figure 12: Web Member Cross-Sections of Aegis Designs.

### 3.3. Specimen Preparation

Aegis truss materials were delivered to the RTF. Members were cut to size and fastened with #10-16 tek screws by undergraduate workers using industry standard practices.



Figure 13: Cold Formed Web Members

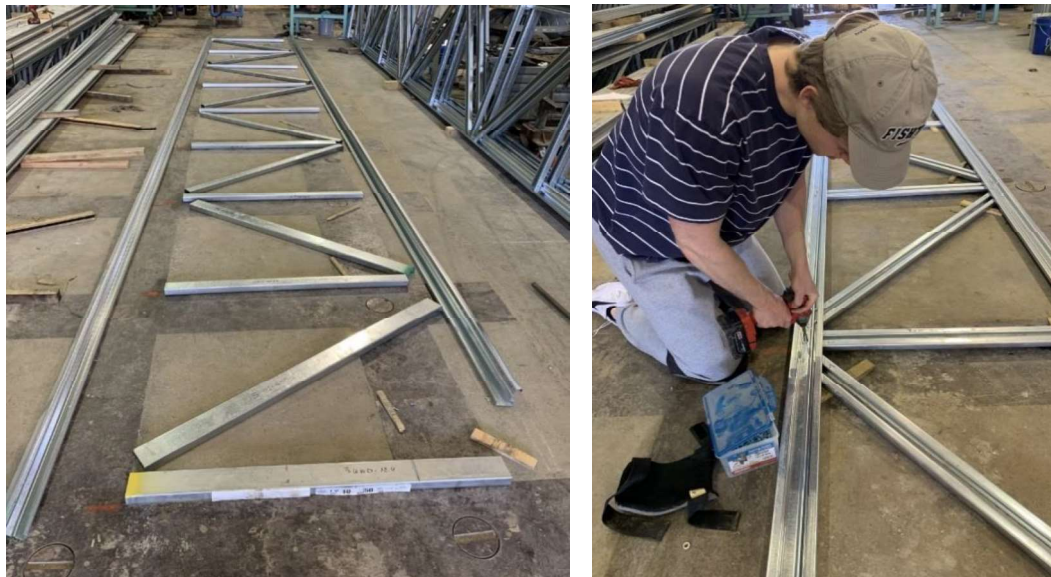


Figure 14: Truss Assembly

Each truss specimen is composed of two trusses placed back-to-back and spaced at a distance of 24 inches from the outside of the chords. 16 gauge hat channel was used as diagonal and lateral bracing and placed at every other panel point according to design drawing to stabilize the specimen during testing and prevent out of plane warping under high deformations (Figure 16). Bracing was fixed to the top and bottom chord members via 3x3x7-1/4" Swiftclip angles as shown in Figure 15. To simulate sheathing, 20 gauge corrugated metal roof decking was attached to the top chord of the specimen with #10-16 tek screws as seen in Figure 16.



Figure 15: Swiftclip Bracing Angles

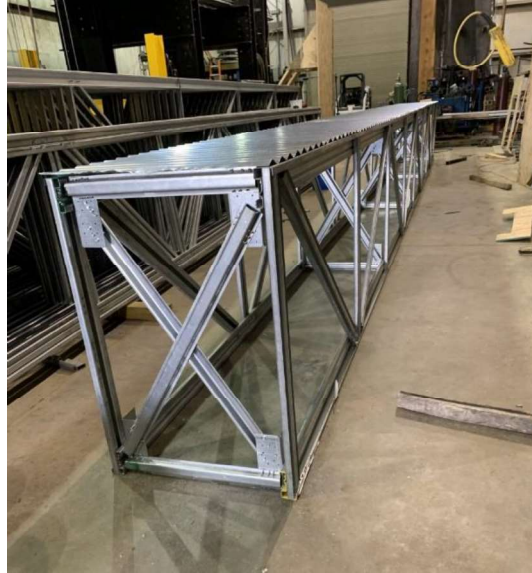


Figure 16: Fully Assembled Specimen

In addition to horizontal and diagonal bracing, three wooden buttresses were placed near quarter points on both sides of the specimen to simulate a lateral restraint. To avoid frictional resistance, 9 inch caster wheels were clamped onto the top and bottom chords to allow the specimen to glide up and down the restraining buttress

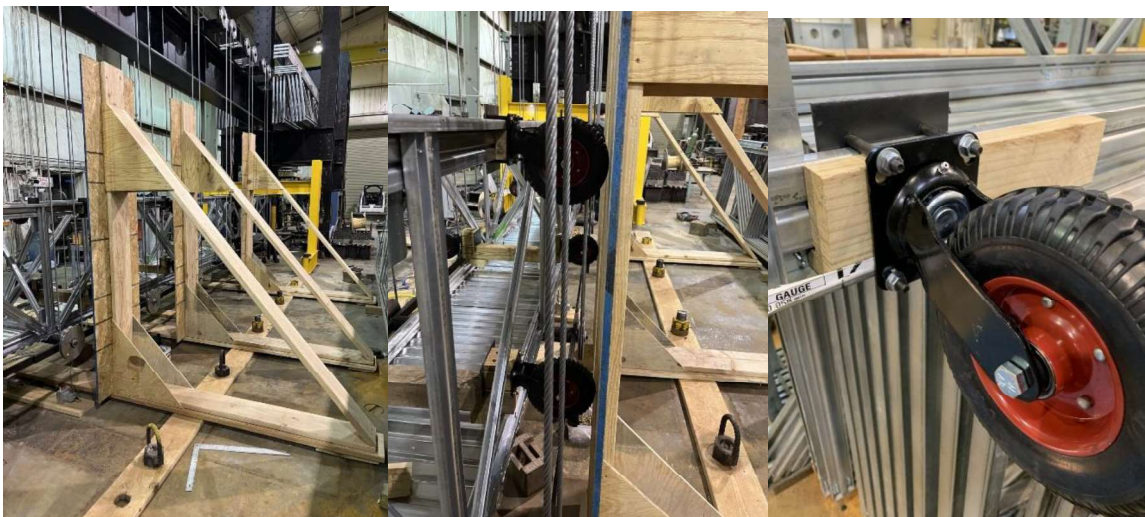


Figure 17: Lateral Restraint System.

Eight strain gauges were installed on chord and web members as shown in Figure 18. Strain gauges were placed strategically to capture strains closest to failure areas. 3 displacement potentiometers were placed along the top chord of the specimen to collect deflection measurements.

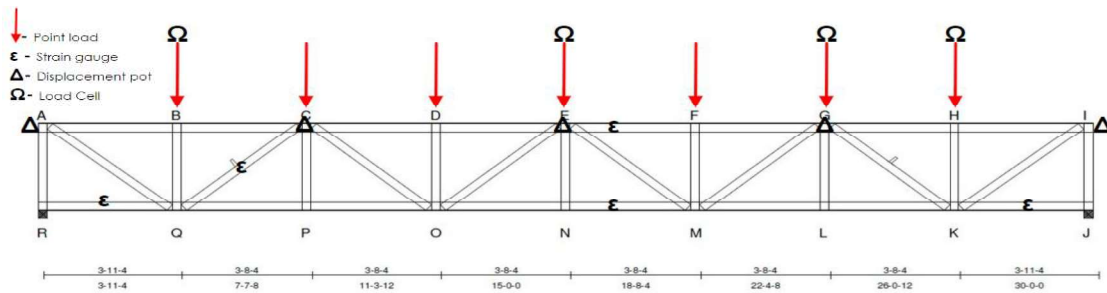


Figure 18: Instrumentation Placement

It is important to note that the specimens are tested upside down. Therefore, during testing the top chord is on the bottom and the bottom chord is on the top. In this paper, the chord position will always be referred to by its design configuration. So, in a positive loading phase, the top chord is the compression chord and the bottom chord is the tension chord. Before load is applied, the instrumentation is zeroed out in the data acquisition box, as well as in the LabVIEW program.

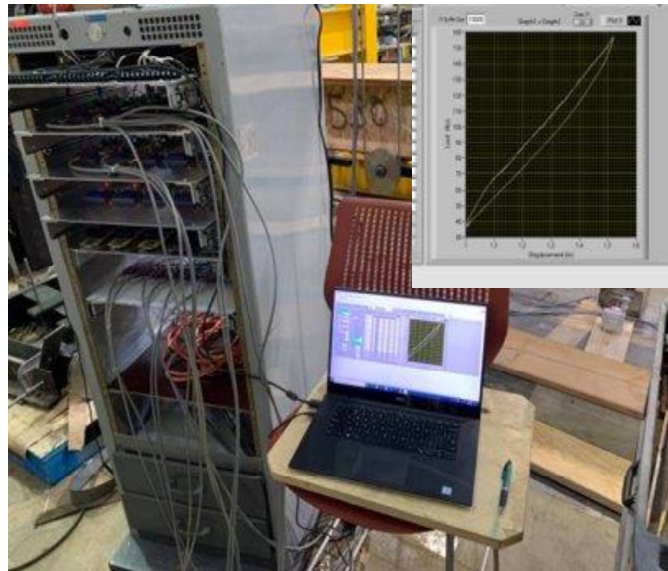


Figure 19: Data Acquisition System

The specimens were connected to the bearing supports with cold-formed clip angles. Four screws fixed the flip angle to the outer flange of the end-vertical element of the truss. The clip angle was then clamped between two steel bolts and fixed to the bottom flange of the supporting as shown (Figure 20). Based on previous research by Bondok and Salim, it was determined that four screws in each bearing connection would provide an appropriate capacity for the connection (Bondok & Salim, 2021). Additional image showing the test setup can be found in Appenix A.



Figure 20: Typical End Bearing Connection

### 3.4. Loading Scenario

Blast waves propagate at supersonic speeds, relative to the speed of sound in air, and are reflected as they meet objects. As the blast wave continues to expand away from the source of the explosion, its intensity diminishes, and its effect on the objects is also reduced.

The air shock wave produces an immediate increase in pressure above the ambient atmospheric pressure at a point some distance from the source. This is commonly referred to as overpressure. Consequently, a pressure differential is generated between the combustion gases and the atmosphere, causing a reversal in the direction of flow, back towards the center of the explosion, known as a negative pressure phase. This is a

negative pressure relative to atmospheric, rather than absolute negative pressure, see Figure 21. Equilibrium is reached when the air is returned to its original state.

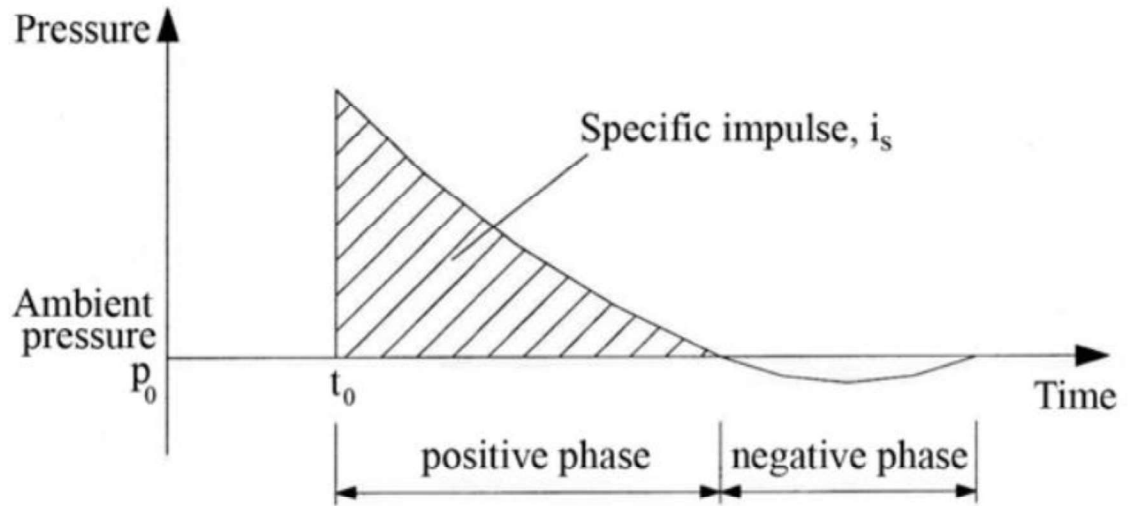


Figure 21: Blast Wave Pressures Plotted Against Time.

A negative pressure phase follows, but it is neglected by most designers since it is much lower in magnitude. In this study, the positive phase effect will be studied by testing the specimens up to failure in the positive phase loading direction.

# 4. Experimental Results

The three specimens considered in this thesis were tested statically up to instability. In all three samples, an initial perfect linear stage was observed, followed by a non-linear stage near peak load, subsequent softening, and decay of capacity up to failure. All joints are referred to by a combination of two letters. The first letter indicates the position of the joint in the configuration and the second, N or S, indicates its residence in the north or south truss. Truss elements are referred to by the two joints on either end. Additional images of the specimen failures can be found in the Appendix B.

## 4.1. AG36-D35

Specimen AG35-D35 demonstrated a bending failure due to global buckling and distortion in the compression chord around the west quarter-span. The specimen had slight global twisting due to more extensive distortion in the south chord, but twisting did not occur until after the truss reached its full capacity. The load maxed out at 10 kips with 3.7 inches of midspan deflection. The specimen continued to deflect until it became unstable at 33 inches of midspan deflection.

### Load vs. Displacement @ 1/2 Span Design #5: AG36-D35

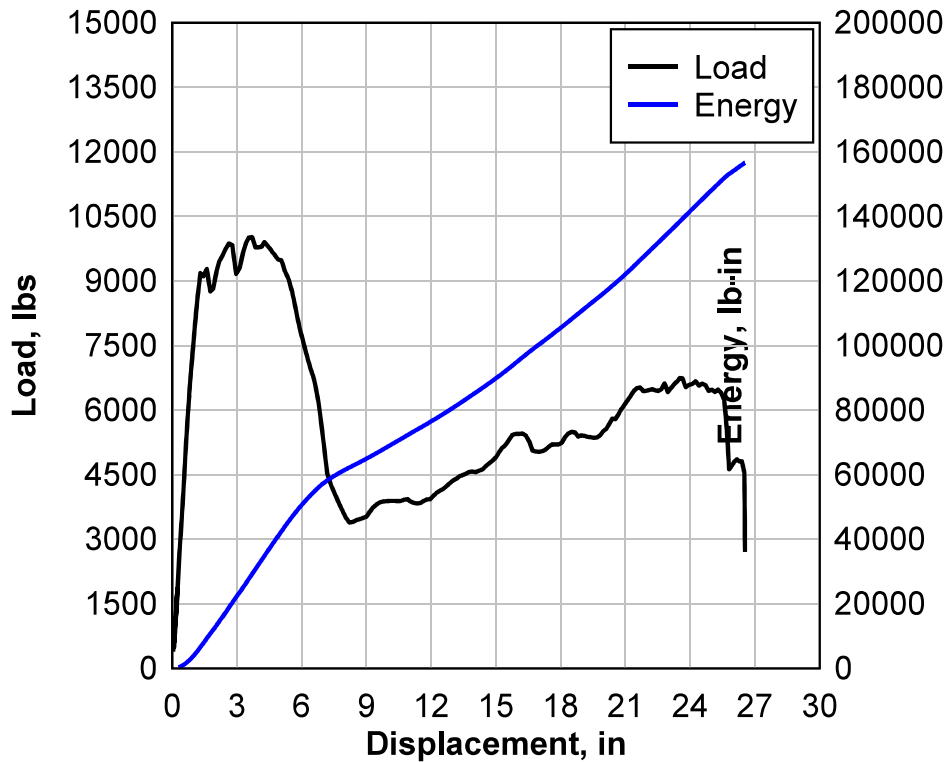


Figure 22: Load vs. Displacement of AG36-D35

After the initial linear stage, oscillating hardening and softening can be observed around peak load as the failure occurred and the load was redistributed. Due to the ductile nature of the failure, the specimen was able to develop some tension membrane action and begin picking up load after the initial failure. About 67% of the peak load was regained before the bearing connections began to fail and the specimen became unstable.

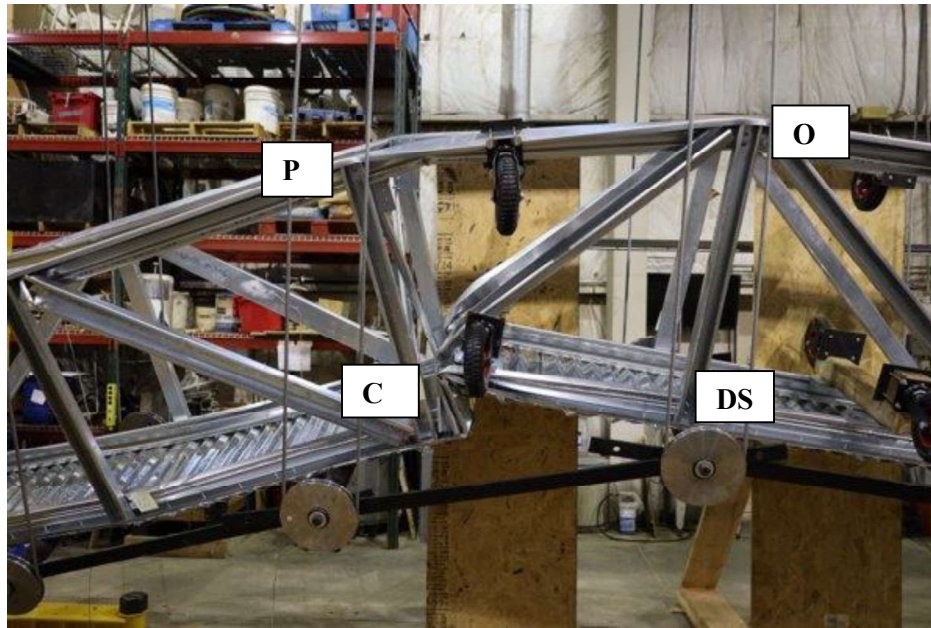


Figure 23: Distortion of Compression Chords in AG36-D35

Failure was initiated by buckling of the compression chord as seen in Figure 23. After chord buckling, the load dropped to 34% of the maximum load. Some deformations due to local buckling were observed in the tension chords at joint Q and the main compression diagonal C-Q. Figure 24 shows the initial deformation of the tension chord at joint Q prior to global failure. Figure 25 shows initial deformation in the compression diagonal C-Q. After compression chord buckling, panel CDOP became distorted due to the excessive deformation of the compression chord, and the tension chord experienced further distortion and bending. Some subsequent twisting of the specimen resulted from the unbalanced distortion of the two compression chords, with the southern chord distorting slightly more than the northern one.

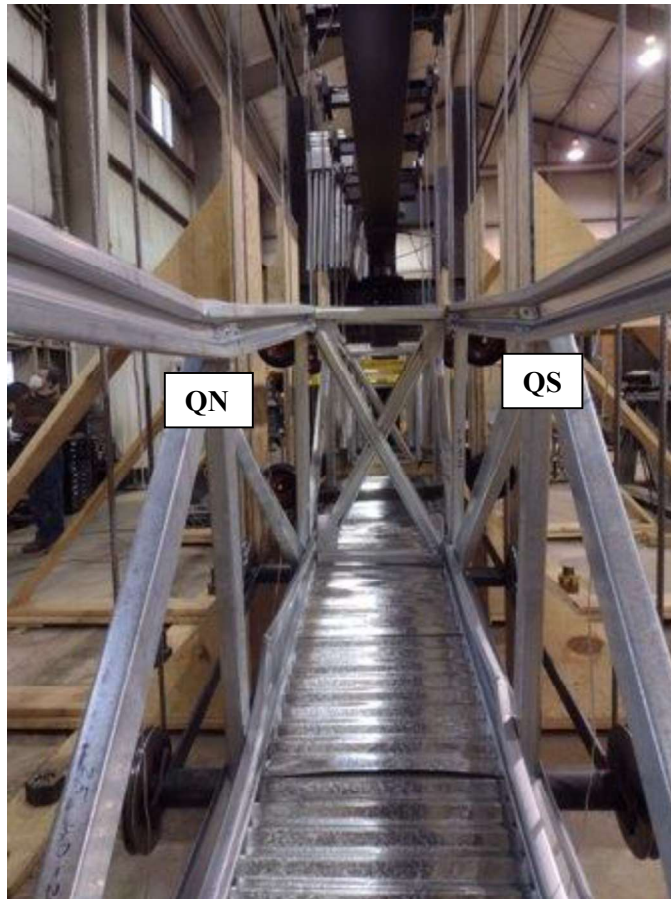


Figure 24: Local Buckling of Tension Chord at Joint Q (AG36-D35)

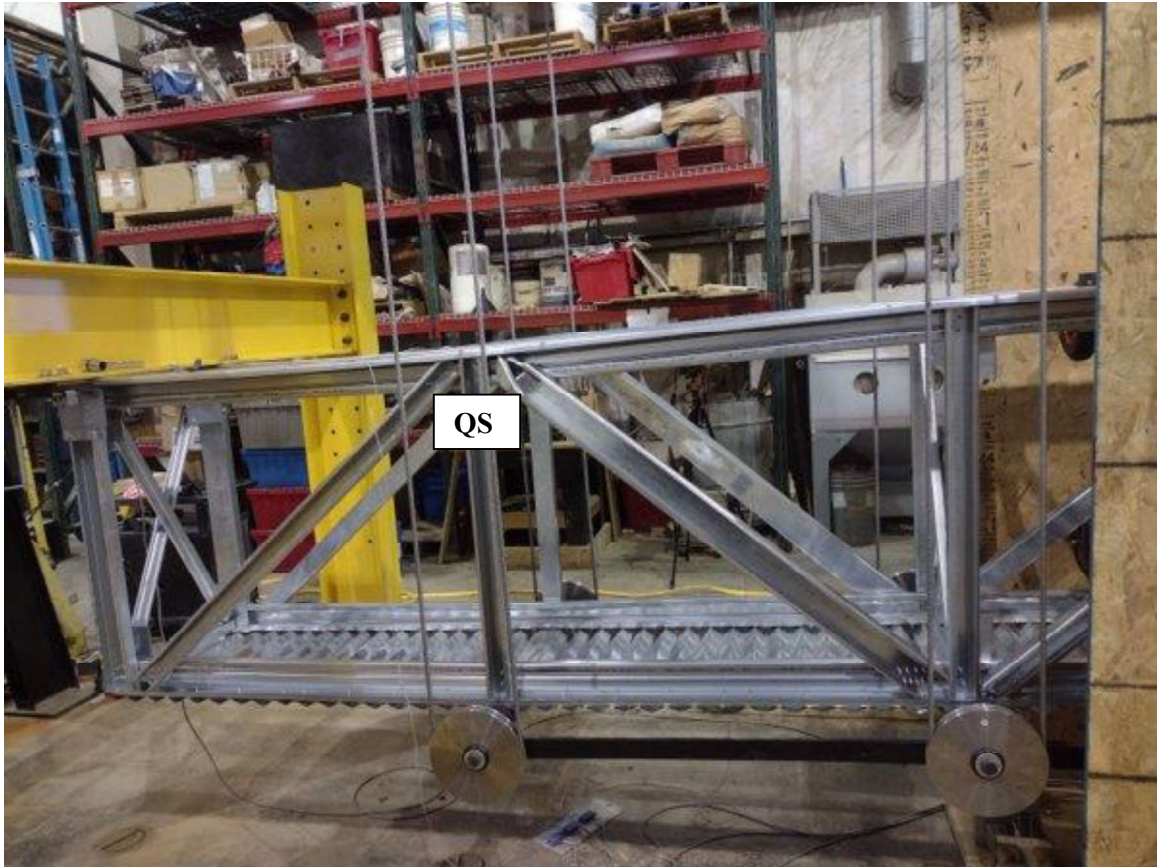


Figure 25: Initial Deformation of Compression Diagonal at Joint QS (AG36-D35)

Other partial failures occurred in some web element connections with the chords such as at joints QN, AN, and PS as shown in Figure 26. Compression in verticals B-Q , A-R, and C-P caused screws to pull out of the vertical elements. Tearing can be seen around the screw holes.



Figure 26: Partial Failures in Web Element Connections (AG36-D35)

Finally, the end bearing connection began to fail at the west end. The connection at RN experienced mixed failure modes of screw shearing and pull-out between the tension chord and vertical A-R as seen in Figure 27. Vertical A-R remained partially connected to the support. Because of the global twisting, the bearing connection at RS, the chord, and vertical members remained partially connected to the deformed clip angle that attached the specimen to the support as shown in Figure 28.

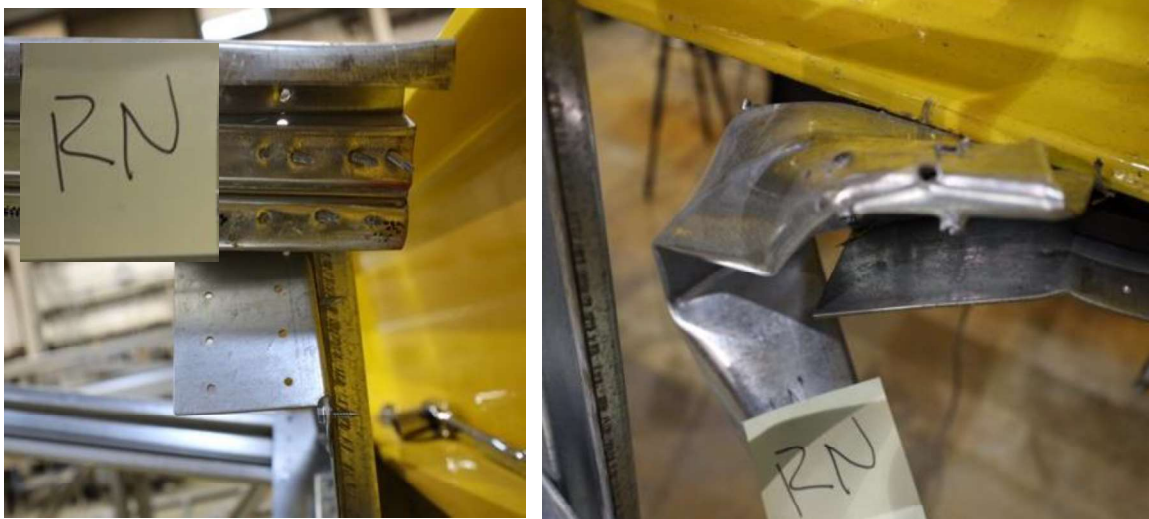


Figure 27: Bearing Connection Failure at RN (AG36-D35)



Figure 28: Bearing Connection at Joint RS (AG36-D35)

## 4.2. AG48-D35

Specimen AG48-D35 failed around the west side at the first panel due to high shear force in the web elements. The tension chords experienced severe local buckling and bending occurred due to continuous upward action restricted by the web elements. Furthermore, tension chord separation at the west end-verticals played a significant role in global failure. Truss action was eliminated after separation causing bending of the compression chord. This led to a full breakage of one chord at the flexure point. Figure 30 shows the global failure of the specimen. The specimen reached a maximum load of 12.3 kips at around 1.2 inches of midspan deflection. After failure, the load dropped to around 36% of

maximum. Resistance increased slightly but then continued to drop until it became unstable. The specimen absorbed up to 125000 lb-in of energy before the test was stopped. Figure 29 shows load and energy vs displacement for the specimen.

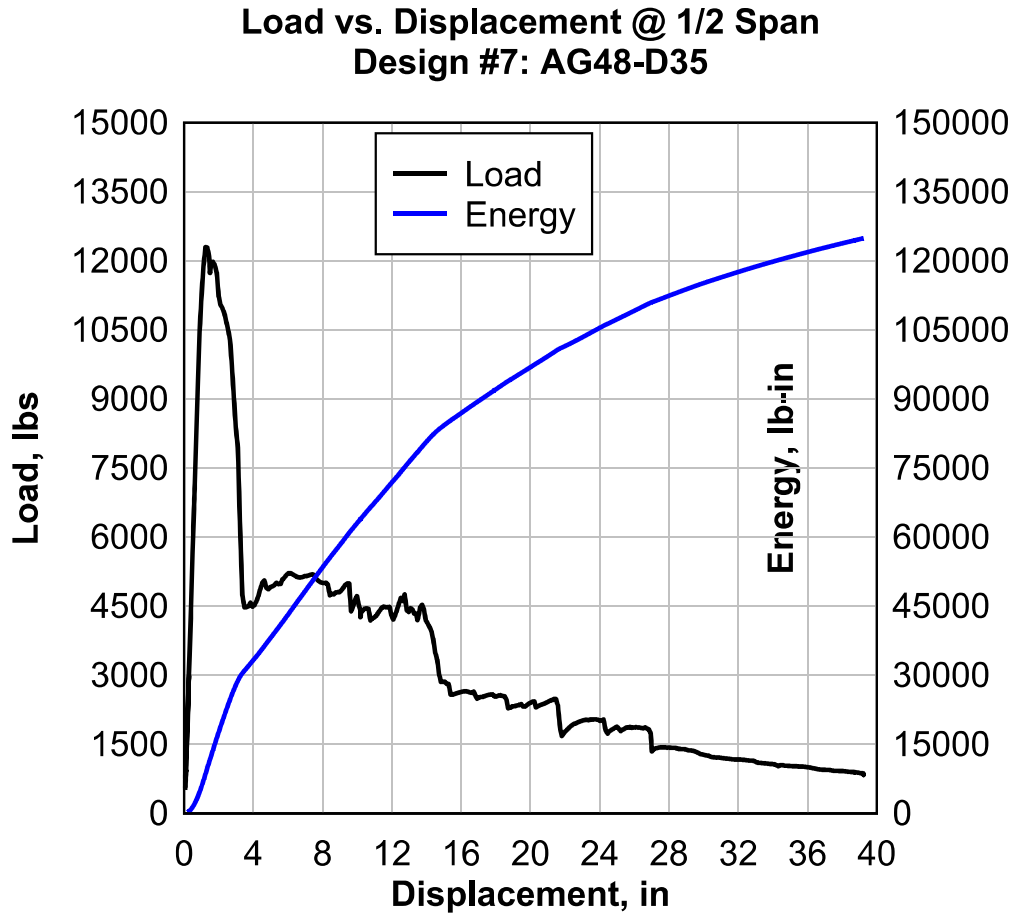


Figure 29: Load and Energy vs Displacement (AG48-D35)



Figure 30: Global Failure of Specimen (AG48-D35)

Failure initiated with the rupture of the main tension diagonal A-Q. the diagonals in both north and south trusses were severely distorted at joint A, along with the end verticals A-R. The diagonals ruptured after cutting began around a screw hole and propagated through the section (Figure 31). It is common for truss element rupture or chord separation to initiate at a screw hole. This is because the chord to web connections did not allow room for adequate screw spacing. While a high number of screws were required for the capacity of the connection, the proximity of screws in some connecton created a least-resistance line of ruptre. Following the web rupture, both tension chords began to separate from the west end verticals, leaving verticals A-R partially connected to the deformed clip angle at the support (Figure 33). Figure 36 shows the west quarter of the specimen during failure, following the rupture of diagonal A-R. The twisting of vertical A-R is evident as the chord attempts to free it from the bearing connection. Local buckling of the compression chord can also be seen at joints A and B before it is bent around the loading bar. The southern compression chord eventually experienced full cutting through the section at join BS. The connection failure between the tension chord the end vertical displayed a mix of screw shearing and pull-out in the 9 screws that

connected the two as shown in Figure 35. After separation, the tension chords were severely bent around joint Q (Figure 32). The strain gauge attached to section QS-RS recorded an obvious jump in tension up to 4000  $\mu\epsilon$ . This was caused by the increased tension in that section as the chord separated from the support. The same chord section on the north truss did not record an equivalent jump in strain. This is because the chord experienced partial tearing through the section at joint QN as shown in Figure 34. As truss deflection increased all screws were eventually sheared in both sides of the East end bearing due to excessive rotation about Joint J.



Figure 31: Rupture of Diagonal at Joint AN (AG48-D35)



Figure 32: Bending of Tension Chords at Joint Q (AG48-D35)

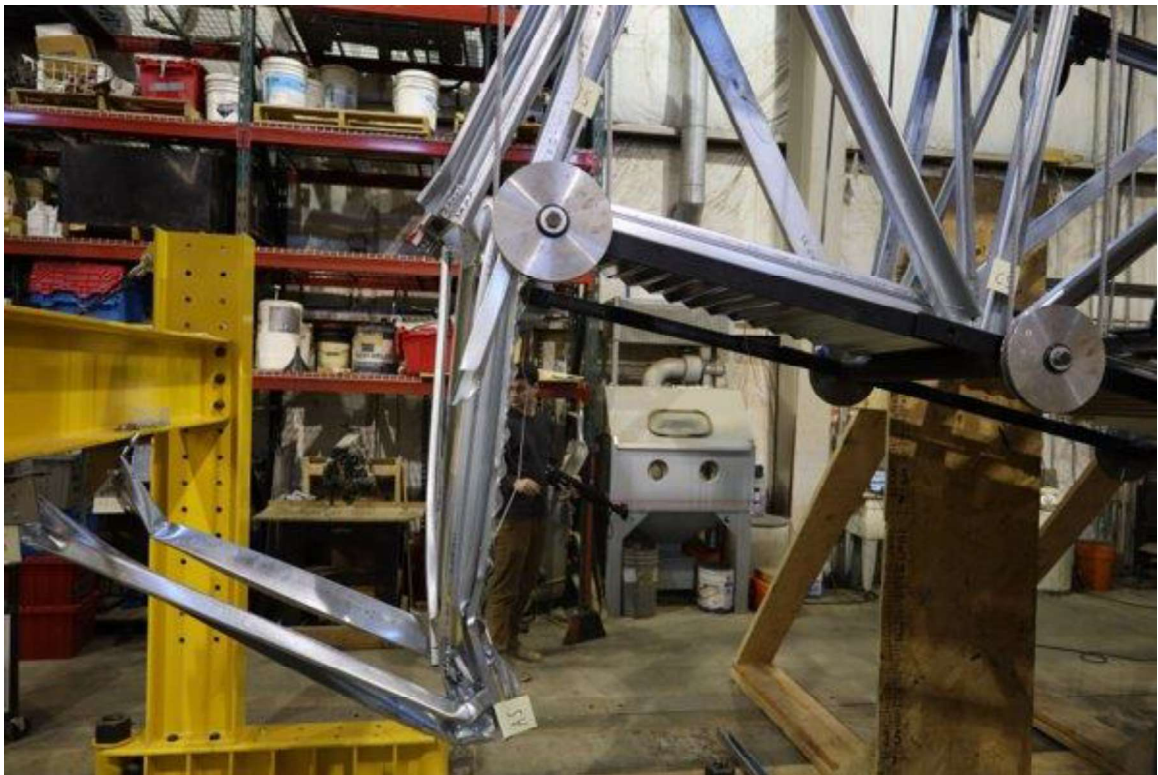


Figure 33: West End Vertical Distortion (AG48-D35)



Figure 34: Partial Tearing in Tension Chord at Joint QN (AG48-D35)



Figure 35: Connection Failure Between Tension Chord and End Vertical at Joint RN (AG48-D35)



Figure 36: West Quarter of Specimen During Failure (AG48-D35)

### 4.3 AG48-D57

Similar to AG48-D35, this specimen failed around the west side with separation in the tension chord and subsequent bending in the compression chord. The load peaked at 14.3 kips around 2.2 inches of deflection. The load then dropped to 60% of maximum, increased slightly, and then dropped to 15% of maximum around 5 inches of midspan deflection. From there, load continued to drop steadily up to ultimate failure. The specimen absorbed about 81500 lb-in of energy before ultimate failure. Figure 37 shows load and energy vs displacement for the specimen. Failure was controlled by high shear in the web elements concentrated near the end of the specimen.

**Load and Energy vs. Displacement @ 1/2 Span  
Design #8: AG48-D57**

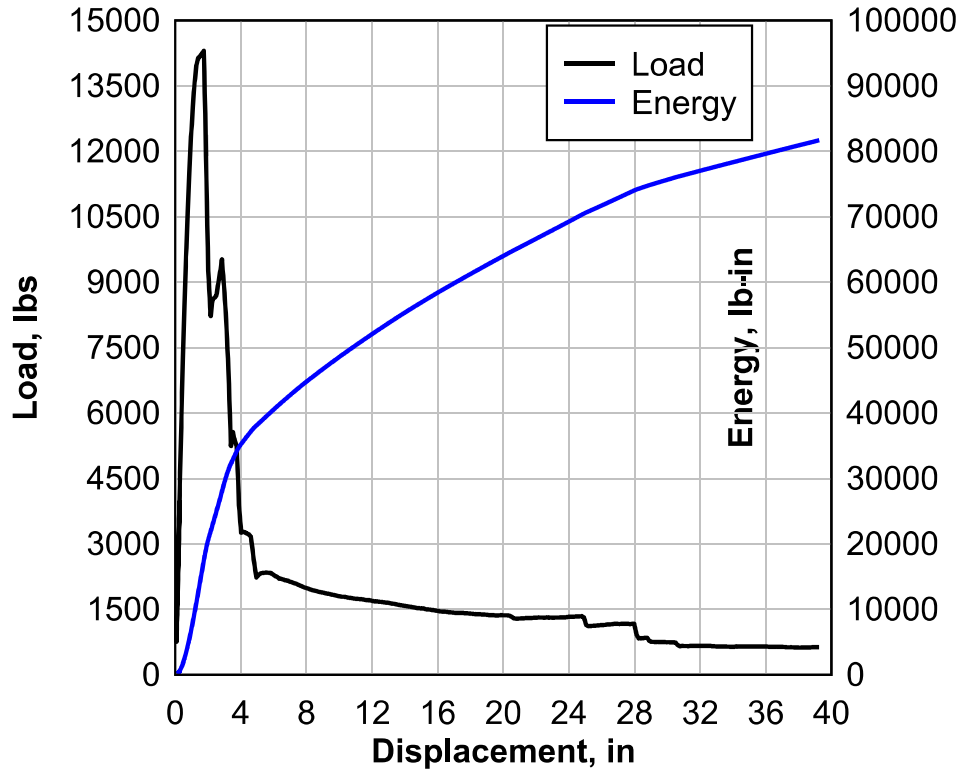


Figure 37: Load and Energy vs Displacement (AG48-D57)



Figure 38: Global Failure of Specimen

Initially, the tension chords displayed some deformation at joint Q caused by the high-tension force in diagonal A-Q (Figure 39). Separation of the tension chords began at joint Q around the connection with diagonal A-Q (Figure 40). The influence of tension chord damage caused a partial failure in the connection with vertical B-Q. A full separation of both tension chords followed nearly simultaneously, eliminating truss action (Figure 41). Figure 42 shows the clear cutting of chord sections caused by the internal shear component from Vertical B-Q and diagonal C-Q. Vertical B-Q was fully separated from the chord and left to dangle. After full separation of the tension chords, the compression chords continued to resist beam action as the only remaining continuous longitudinal elements. Bearing at both ends of the specimen continued to effectively constrain longitudinal movement, causing the compression chords to severely bend at joint C under continued loading as seen in Figure 43. The global deformation also caused a partial deformation of both connecting web elements at joint A. Excessive rotation of the specimen at both the east and west end caused a clear shear failure in the end bearing connection. The failure happened at all four screws connecting the chord with the clip angle.



Figure 39: Initial Tension Chord Deformation (AG48-D57)



Figure 40: Beginning of Tension Chord Separation (AG48-D57)



Figure 41: Full Tension Chord Separation



Figure 42: Cutting of Tension Chord Section (AG48-D57)



Figure 43: Compression Chord Bending (AG48-D57)

#### 4.4. Parametric Study

Three specimens were considered in this paper. All three had the same section types and construction methods. Two had the same height, but different section thicknesses.

Another two had the same section thicknesses, but different heights. Table 2 shows parametric data for the three specimens.

Table 2: Parametric Data

<b>SPECIMEN</b>	<b>ELEMENT THICKNESS</b>	<b>HEIGHT</b>	<b>WEIGHT</b>	<b>PEAK LOAD</b>	<b>ENERGY</b>
	(in)	(in)	(lbs)	(kips)	(lb-in)
<b>AG36-D35</b>	0.035	36	248	10	156555
<b>AG48-D35</b>	0.035	48	278	12.3	124881
<b>AG48-D57</b>	0.057	48	332	14.3	81620

The sample with the highest energy absorption was also the sample with the lowest peak load. Interestingly, the two 48 in. specimens both failed due to the separation of the tension chord, and very little deformation occurred in the elements. The sudden cutting of truss elements caused a brittle failure and leaves little opportunity for the truss to pick up more load after it is dropped. In both cases, truss action was eliminated immediately after chord separation, and the truss was reduced to the bending capacity of the compression chords alone. Therefore, as seen in Figure 44, AG48-D35 and AG48-D57 drop load after initial failure and continue to drop load up to ultimate failure.

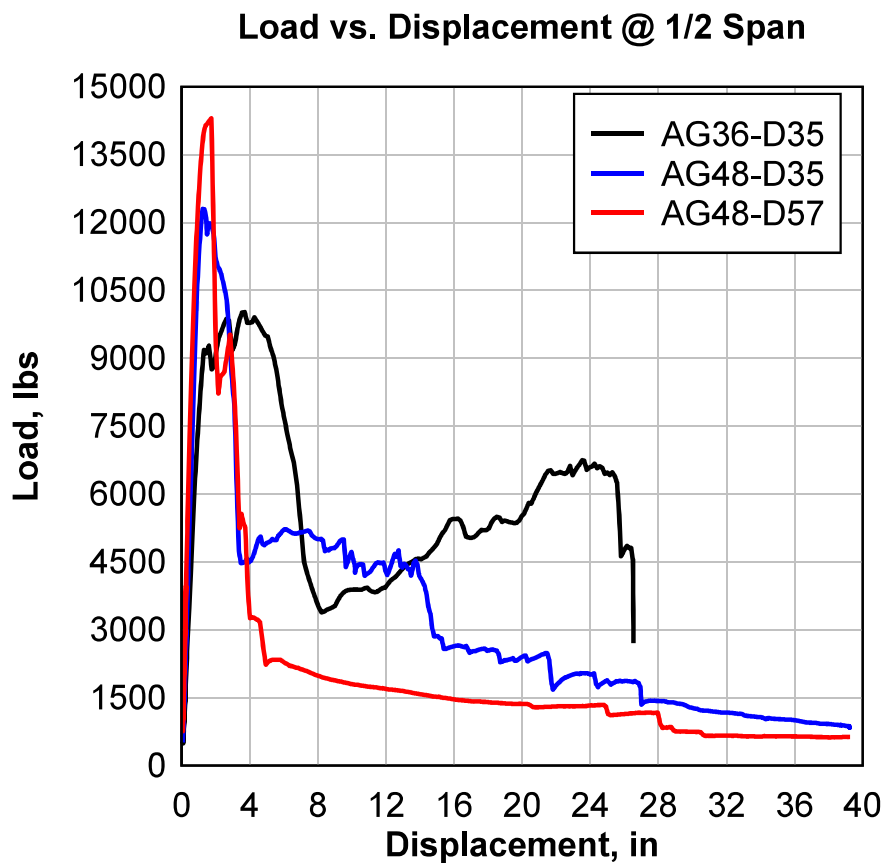


Figure 44: Load vs Displacement Comparison.

AG36-D35 was able to regain up to 51% of the dropped load by developing tension membrane action. Recall, specimen AG36-D36 experienced major buckling of the compression chord, as well as local buckling in the tension chords and some web elements. Buckling of elements releases high amounts of energy and allows the truss to continue building load capacity. After buckling, the truss behaves like a rope, carrying load under high deflection as long as the bearing connection remains secure. When the bearing connection failed, the tension action was eliminated and the load dropped sharply up to ultimate failure as seen in Figure 44. This is why AG36-D35, the specimen with the lowest peak load, absorbs the most energy of the three specimens, as seen in Figure 45. In fact, despite weighing 25% less than AG48-D57 and sustaining a peak load of only 70%, AG36-D35 absorbed 92% more energy before ultimate failure.

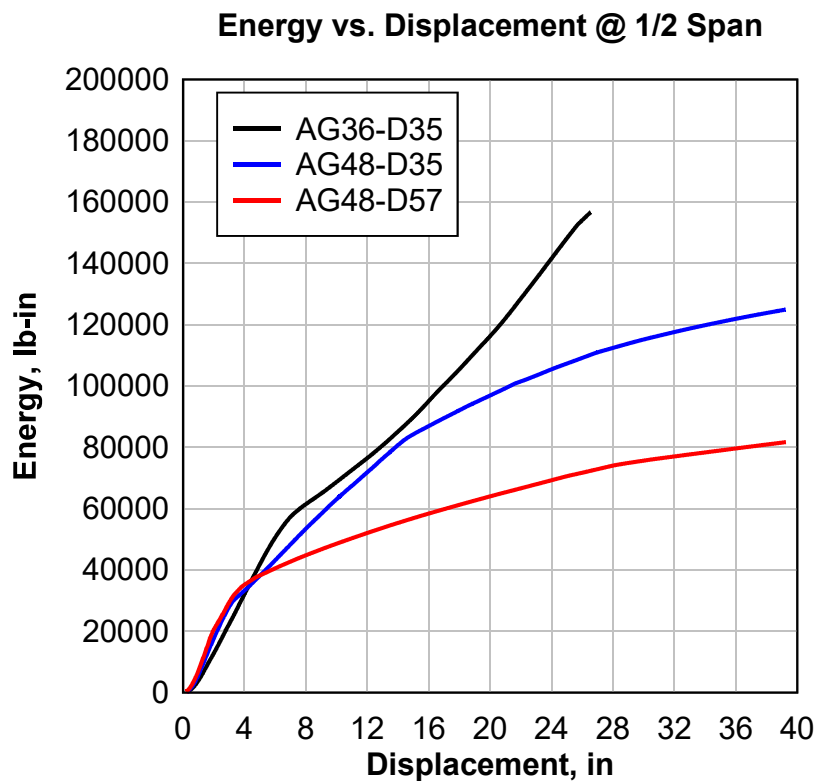


Figure 45: Energy vs Displacement Comparison



# 6. Conclusion and Recommendations

In this thesis, the load-displacement response of full-scale cold-formed steel trusses were evaluated under quasistatic loading. The experimental resistance function of the trusses evaluated was recorded until failure. The various failure mechanisms were observed. The main conclusions and recommendations based on this research are presented next.

## 6.1. Conclusion

Three different CFS truss designs were tested under quasi-static loading up to ultimate failure. Cold-formed steel members demonstrated an excellent performance and ductility under high static loads. The static resistance functions were determined for all specimens. Several different partial and full failure modes were observed during testing, including

- Buckling of structural elements
- Connection Separations
- Rupture of some elements at connections
- Membrane failure
- Tension chord separation

Some general observations regarding the performance of CFS trusses under static load are given as follows:

- Truss capacity is greatly affected by small changes in configuration, section thickness, and geometry.
- End-bearing connections affect the overall response of the CFS truss system.

- Trusses that experience buckling in chord and web elements are able to absorb more energy and regain more load after initial failure than those that experience element rupture or chord separation.

A new mechanical system for static testing was successfully developed and implemented in order to test a wide variety of truss geometries up to high loads with a single loading source. The mechanism achieved a displacement-controlled loading condition.

## 6.2. Recommendations

More work must be done to achieve the goal of developing design methodologies for blast resistance design of CFS roof truss systems. Future work on the subject includes:

- Develop nonlinear finite element models and validate with the results of these experiments
- Develop analytical model for determining static resistance functions of CFS trusses
- Incorporate analytical model into an engineering-level blast design method
- Perform dynamic field testing to verify numerical modeling and analytical tools

One benefit of testing common industry truss designs is the ability to evaluate the failure modes and performance of proprietary designs and section geometries. Recommendations for improving Aegis truss designs are as follows:

- The non-symmetry of Aegis chord sections means that web elements are connected to chords with a single shear plane. The single shear plane means that more screws are required to achieve adequate connection capacity and the chord elements are vulnerable to torsional distortions. I recommend using symmetric chord sections that utilize a double shear plane for chord to web connections
- The high number of screws in the web to chord connections does not allow for adequate spacing between screws. Close proximity of screws creates a least-resistance rupture line across the connected element and makes web elements vulnerable to tension rupture

# 7. References

- Biggs, J. M. (1964). *Introduction to Structural Dynamics*. McGraw-Hill.
- Bondok, D., Clayton, G., & Salim, H. (2018). *Dynamic Response of Roof Truss Systems under Blast Loading*.
- Bondok, D., & Salim, H. (2021). Failure capacities of cold-formed steel roof trusses end-connections. *Thin-Walled Structures*, 171.
- Bondok, D., Salim, H., & Ugresa, G. (2021). Quasi-static Responses and Associated Failure Mechanisms of Cold-formed Steel Roof Trusses. *Engineering Structures*, 231.
- Clayton, G. (2017). “Dynamic Response of Cold-Formed Steel Roof Trusses Subject to Blast Load.” M.S. Thesis, Department of Civil Engineering, University of Missouri, Columbia, MO
- Esper, P. (2004). “Performance of buildings under blast loading and recommended protective measures. In P. Esper (Ed.), *Proceedings of the International Symposium on Network and Center-Based Research for Smart Structures Technology and Earthquake Engineering*.
- Gannon C. J., Marchand, K. A., & Williamson, E. B. (2012). Approximation of blast loading and single degree-of-freedom modelling parameters for long span girders. *WIT Transactions on State of the Art in Science and Engineering*, 60(1755–8336).
- McClendon, M. (2007). “Blast Resistant Design for Roof Systems.” M.S. Thesis, Department of Civil Engineering, University of Missouri, Columbia, MO
- Nourzadeh, D., Humar, J. M., & Braimah, A. (2017). Response of roof beams in buildings subject to blast loading: Analytical treatment. *Engineering Structures*, 138, 50–62. <https://doi.org/10.1016/j.engstruct.2017.02.009>
- Unified Facilities Criteria (UFC) 3-340-02S. (2014). Structures to Resist the Effects of Accidental Explosions. *U.S. Department of Defense, Washington DC*.
- Xiao, W., Andrae, M., Steyerer, M., & Gebbeken, N. (2021). Investigations of blast loads on a two-storeyed building with a gable roof: Full-scale experiments and numerical study. *Journal of Building Engineering*, 43. <https://doi.org/10.1016/j.job.2021.103111>

# Appendix A – Loading Mechanism



Figure 46: Specimen Setup - Longitudinal View



Figure 47: Specimen Setup - Plan View



Figure 48: Specimen Setup - Quarter Span



Figure 49: Specimen Setup - End Panel



Figure 50: Specimen Setup - End Bearing



Figure 51: Compression Cord Sheathing



Figure 52: #10-16 Tek Screws



Figure 53: Hat Channel for Bracing



Figure 54: Displacement Potentiometer Placement

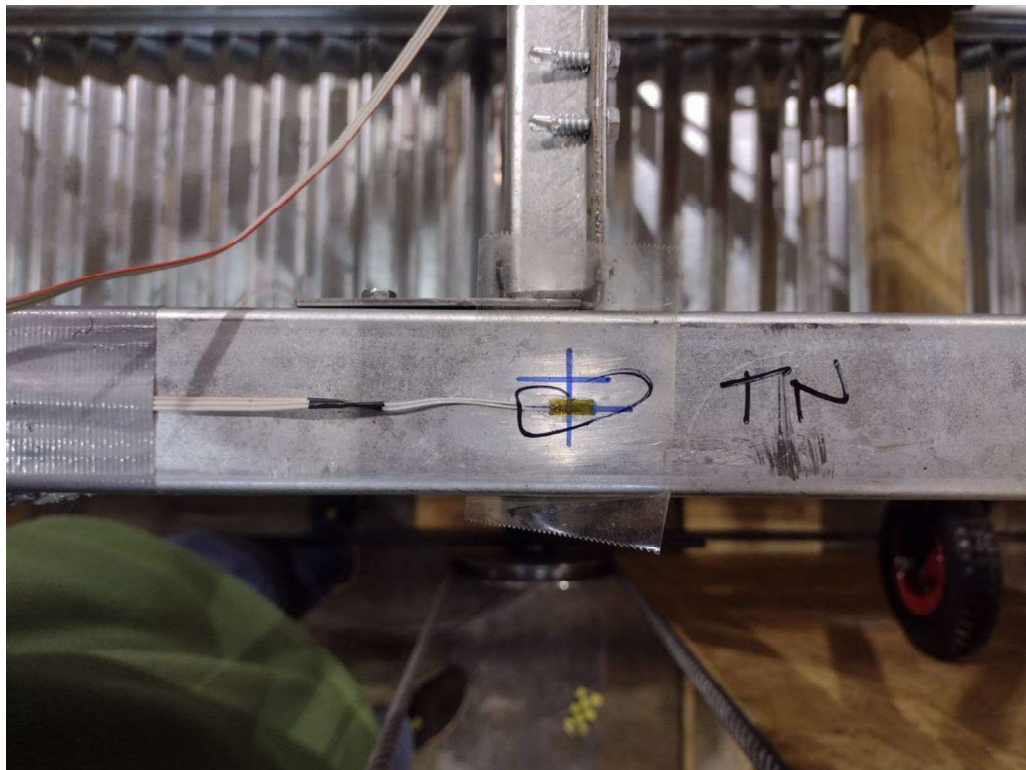


Figure 55: Straining Gauge Placement



Figure 56: Pulley and Cable Elevation View



Figure 57: Caster Wheel Placement Elevation

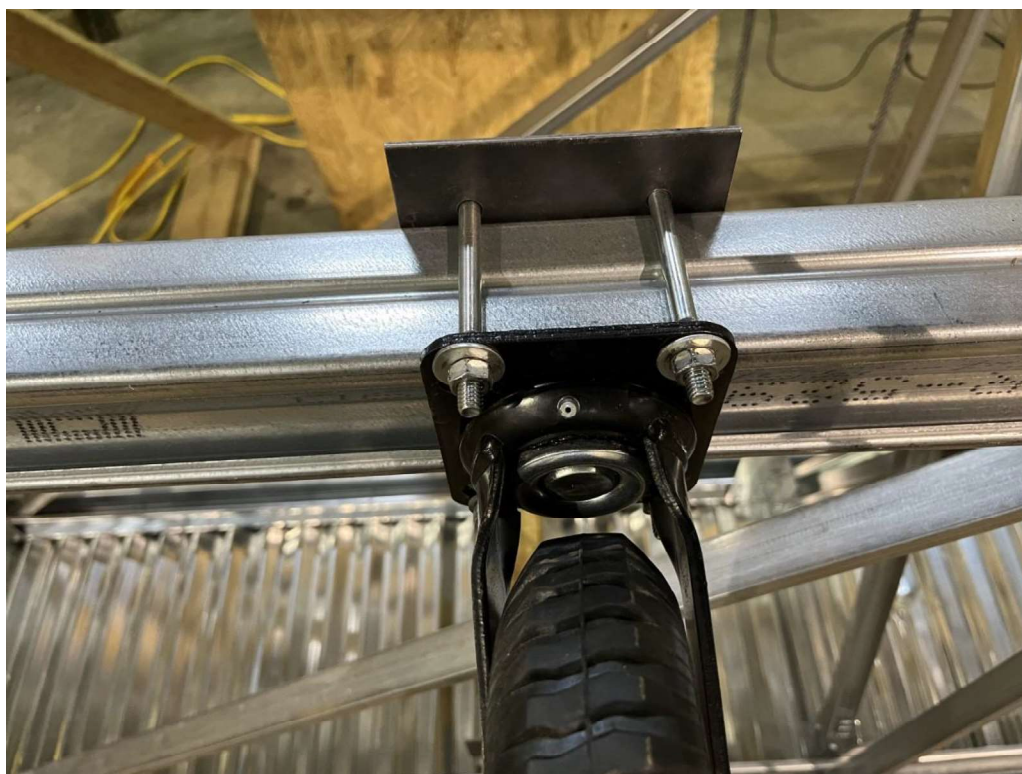


Figure 58: Caster Wheel Placement Plan

# Appendix B – Additional Test Results

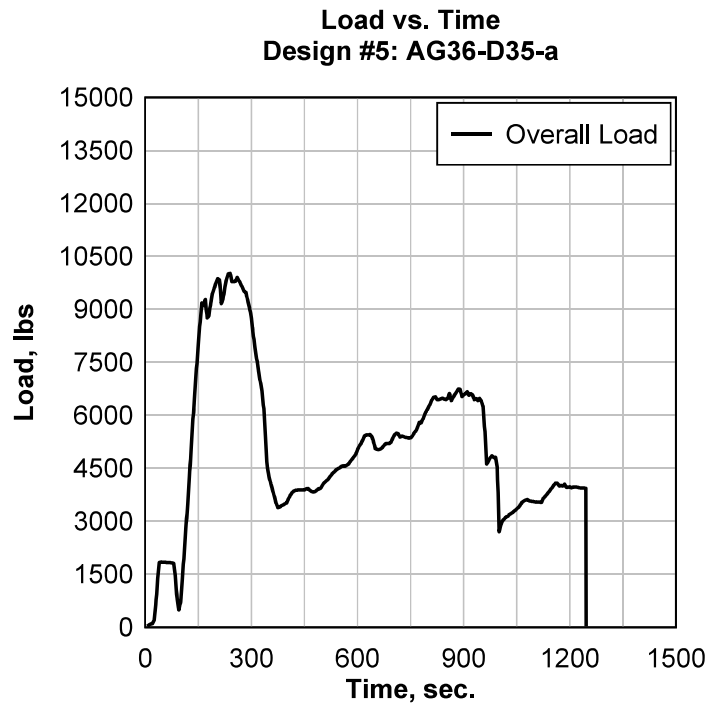


Figure 59: *Load vs Time (AG36-D35)*

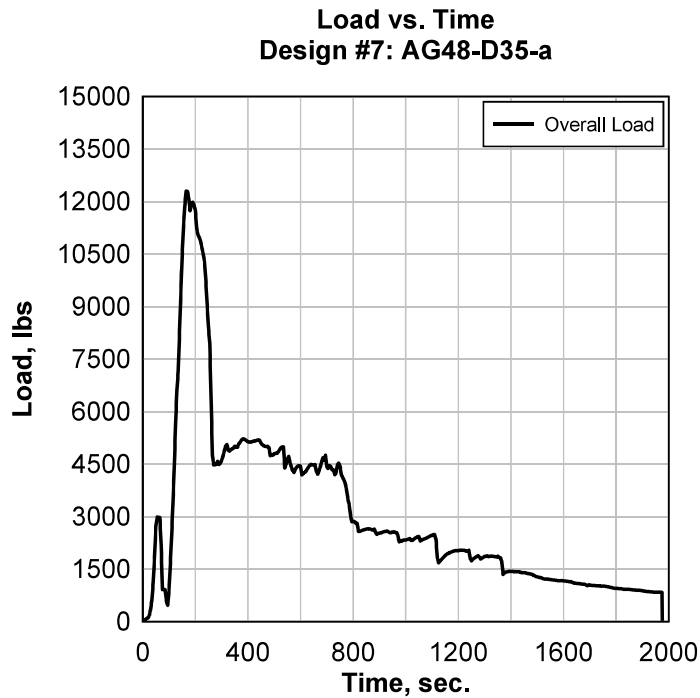


Figure 60: *Load vs Time (AG48-D35)*

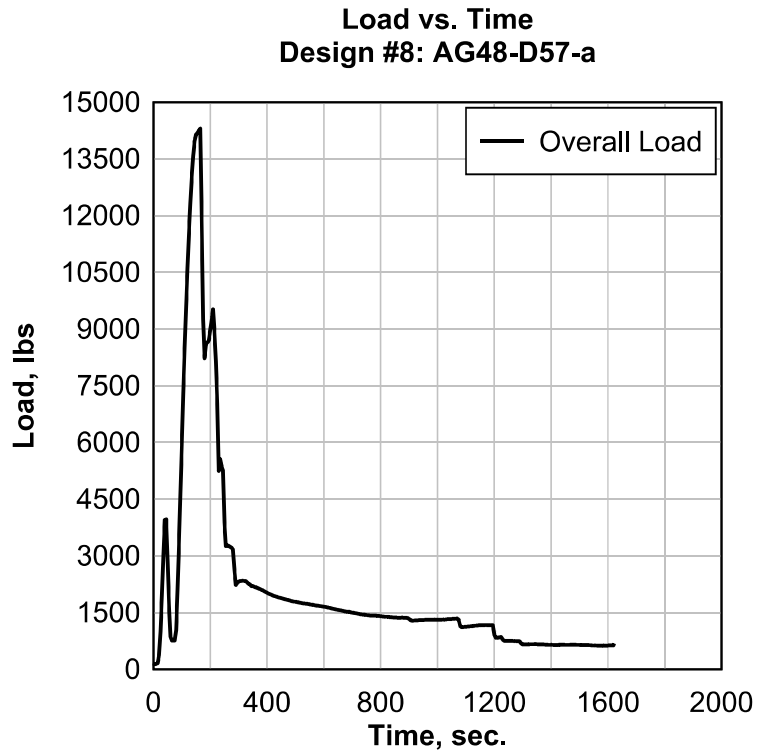


Figure 61: Load vs Time (AG48-D57)

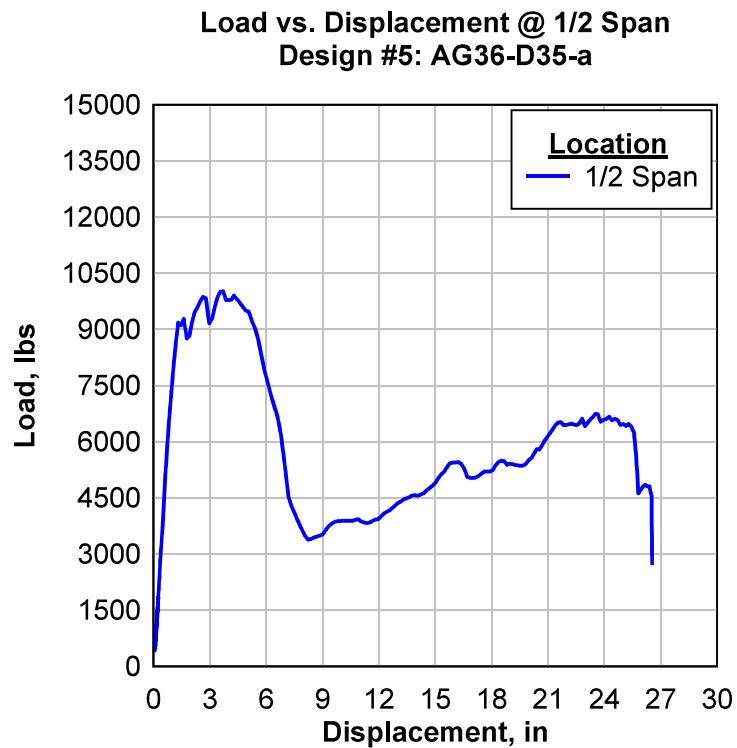


Figure 62: Load vs Displacement (AG36-D35)

Load vs. Displacement @ 1/2 Span  
Design #7: AG48-D35-a

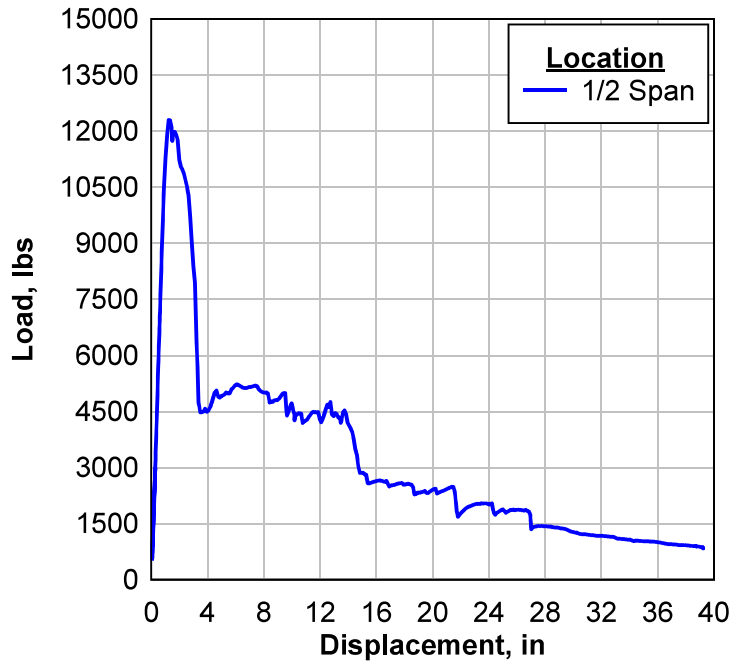


Figure 63: Load vs Displacement (AG48-D35)

Load vs. Displacement @ 1/2 Span  
Design #8: AG48-D57-a

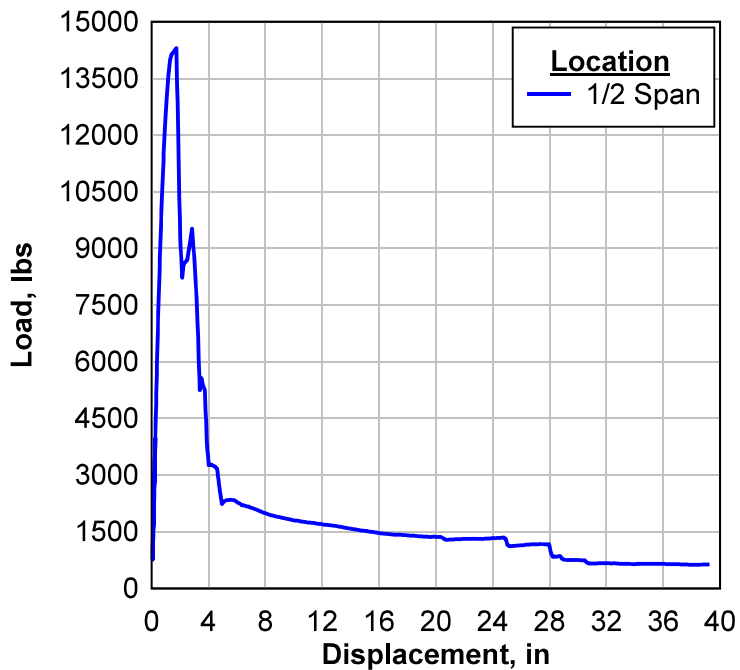


Figure 64: Load vs Displacement (AG48-D57)

**Load vs. Energy @ 1/2 Span  
Design #5: AG36-D35**

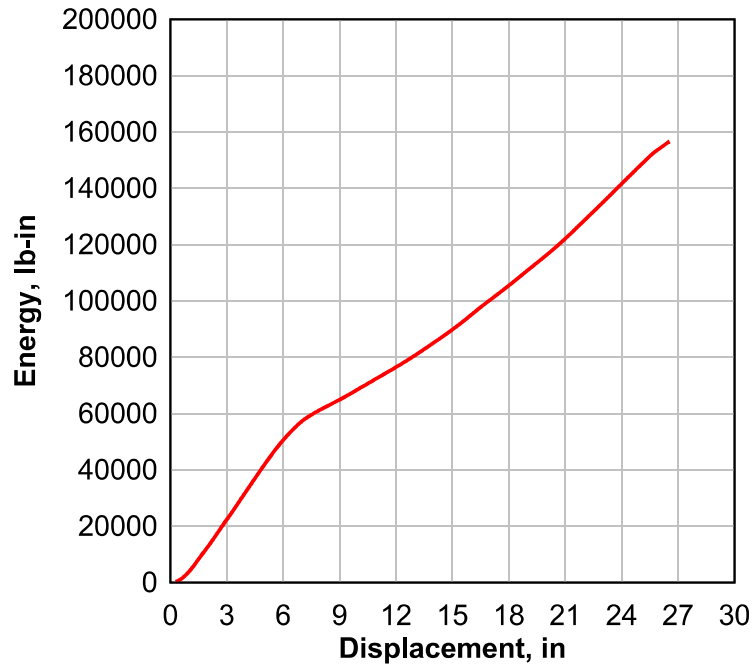


Figure 65: Load vs Energy (AG36-D35)

**Load vs. Energy @ 1/2 Span  
Design #7: AG48-D35**

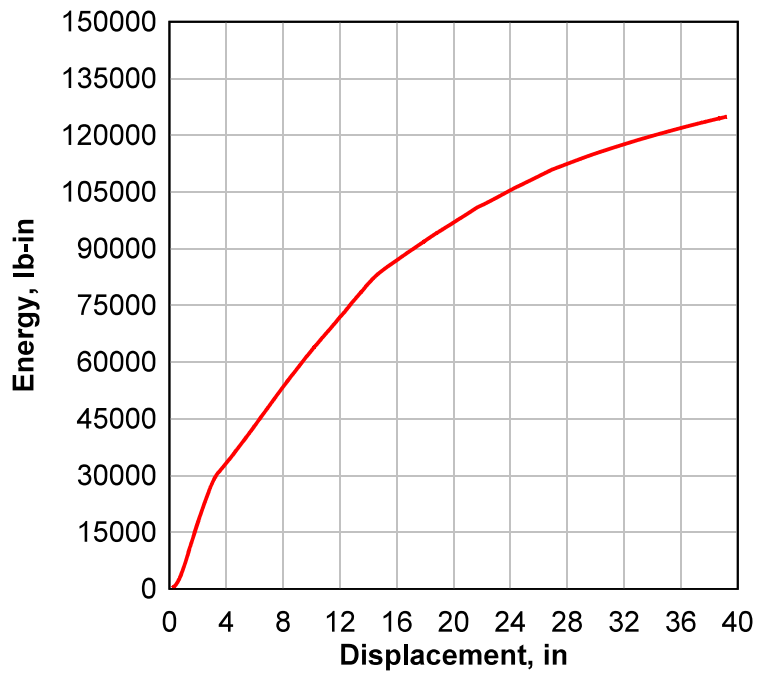


Figure 66: Load vs Energy (AG48-D35)

Load vs. Displacement @ 1/2 Span  
Design #8: AG48-D57-a

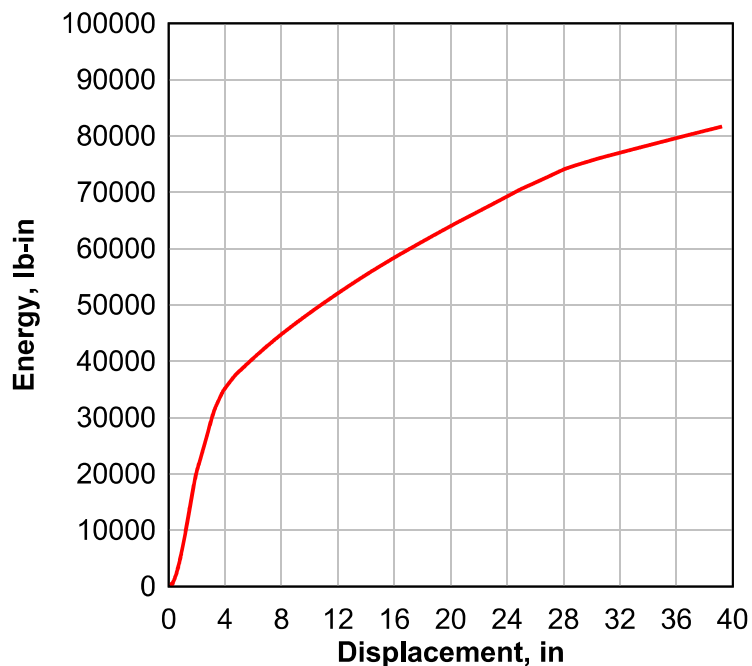


Figure 67: Load vs Energy (AG48-D57)

Load vs. Strain  
Design #5: AG36-D35-a

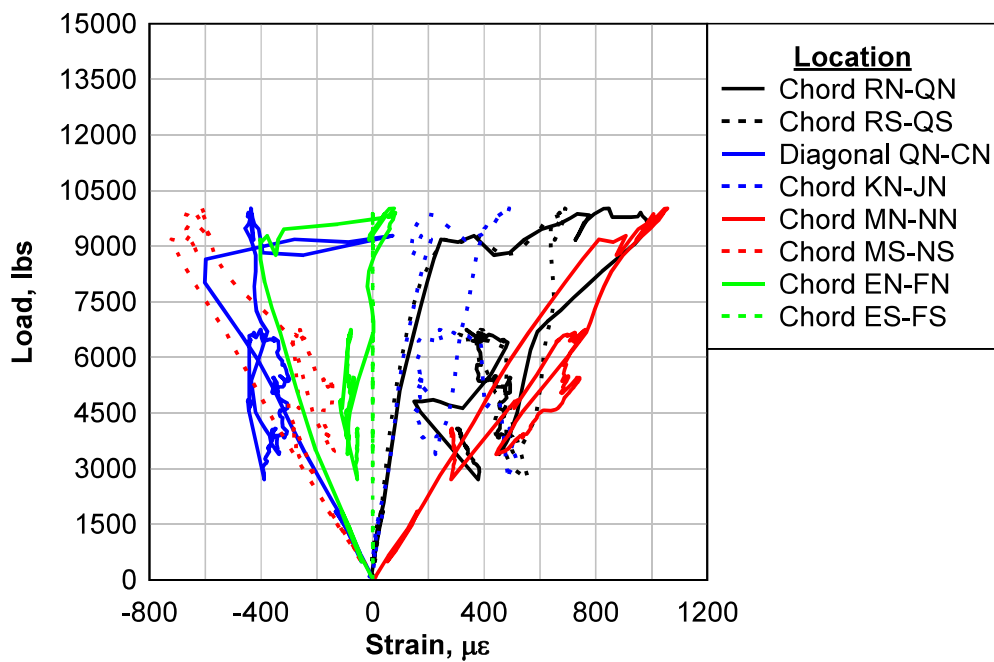


Figure 68: Load vs Strain (AG36-D35)

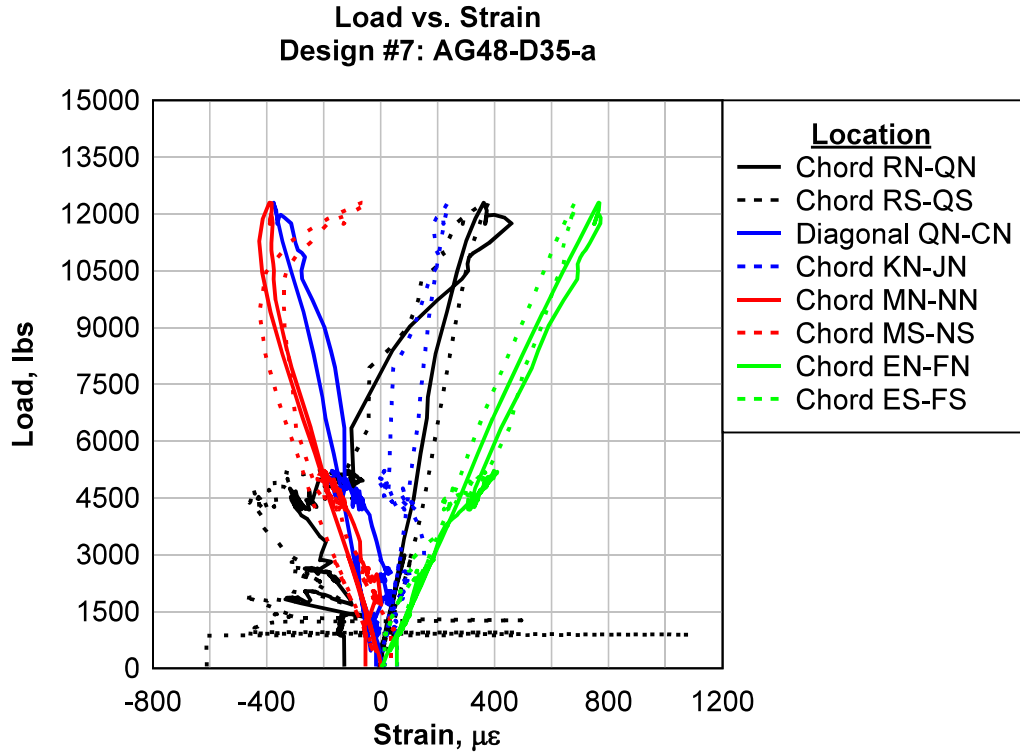


Figure 69: Load vs Strain (AG48-D35)

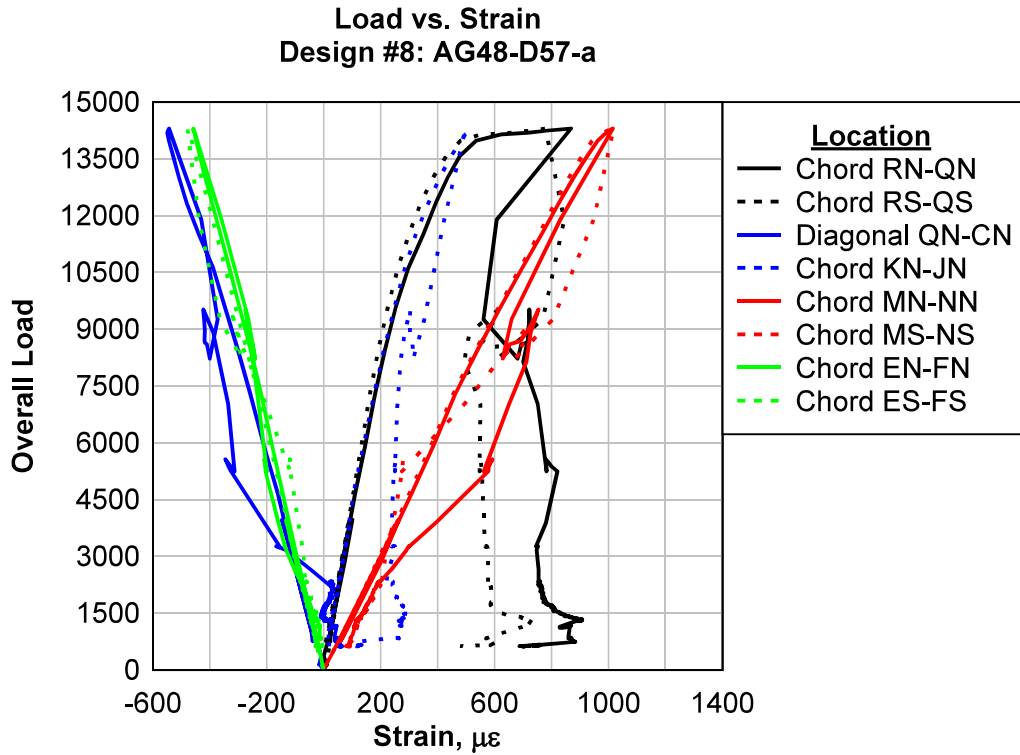


Figure 70: Load vs Strain (AG48-D57)